Inorg. Chem. **2003**, *42*, 2227–2241

Unusual Aryl–Porphyrin Rotational Barriers in Peripherally Crowded Porphyrins

Craig J. Medforth,*,†,‡ Raid E. Haddad,§ Cinzia M. Muzzi,† Neal R. Dooley,† Laurent Jaquinod,† David C. Shyr,† Daniel J. Nurco,† Marilyn M. Olmstead,† Kevin M. Smith,*,†,|| Jian-Guo Ma,§ and John A. Shelnutt*,‡,⊥

Department of Chemistry, University of California, Davis, California 95616, Biomolecular Materials and Interfaces Department, Sandia National Laboratories, Albuquerque, New Mexico 87185, Department of Chemistry and Department of Chemical and Nuclear Engineering, University of New Mexico, Albuquerque, New Mexico 87131, Department of Chemistry, Louisiana State University, Baton Rouge, Louisiana 70803, and Department of Chemistry, University of Georgia, Athens, Georgia 30602

Received September 7, 2001

Previous studies of 5,10,15,20-tetraarylporphyrins have shown that the barrier for *meso* aryl–porphyrin rotation ($\Delta G^{\ddagger}_{ROT}$) varies as a function of the core substituent M and is lower for a small metal (M = Ni) compared to a large metal (M = Zn) and for a dication (M = $4H^{2+}$) versus a free base porphyrin (M = 2H). This has been attributed to changes in the nonplanar distortion of the porphyrin ring and the deformability of the macrocycle caused by the core substituent. In the present work, X-ray crystallography, molecular mechanics (MM) calculations, and variable temperature (VT) ^{1}H NMR spectroscopy are used to examine the relationship between the aryl–porphyrin rotational barrier and the core substituent M in some novel 2,3,5,7,8,10,12,13,15,17,18,20-dodecaarylporphyrins (DArPs), and specifically in some 5,10,15,20-tetraaryl-2,3,7,8,12,13,17,18-octaphenylporphyrins (TArOPPs), where steric crowding of the peripheral groups always results in a very nonplanar macrocycle. X-ray structures of DArPs indicate differences in the nonplanar conformation of the macrocycle as a function of M, with saddle conformations being observed for M = Zn, 2H or M = $4H^{2+}$ and saddle and/or ruffle conformations for M = Ni. VT NMR studies show that the effect of protonation in the TArOPPs is to increase $\Delta G^{\ddagger}_{ROT}$, which is the opposite of the effect seen for the TArPs, and MM calculations also predict a strikingly high barrier for the TArOPPs when M = $4H^{2+}$. These and other findings suggest that the aryl–porphyrin rotational barriers in the DArPs are closely linked to the deformability of the macrocycle along a nonplanar distortion mode which moves the substituent being rotated out of the porphyrin plane.

Introduction

Recent investigations of peripherally crowded porphyrins (e.g., **1**−**5**, Figure 1) have helped to delineate the relationship between the substituents on the porphyrin ring and the amount and type of nonplanar deformation induced by those substituents.[1] Figure 2 illustrates the four nonplanar deformations commonly observed in crystallographic studies of porphyrins.[2] Significant changes in the properties of the porphyrin macrocycle (e.g., redox behavior and photophysics) are now known to result from two types of nonplanar deformation (ruffling or saddling).[1,3,4] These findings have lead to speculation about the role of the nonplanar deformations seen for tetrapyrroles in biological systems,[3] and to investigations of how peripheral crowding might be used to

* Authors to whom correspondence should be addressed. E-mail: medforth@chem.ucdavis.edu (C.J.M.); kmsmith@lsu.edu (K.M.S.); jasheln@unm.edu (J.A.S.).
† University of California.
‡ Sandia National Laboratories.
§ University of New Mexico.
|| Louisiana State University.
⊥ University of Georgia.

(1) For a recent review of nonplanar porphyrins see: Senge, M. O. In *The Porphyrin Handbook*; Kadish, K. M., Smith, K. M., Guilard, R., Eds.; Academic Press: Boston, 2000; Vol. 1; p 239.
(2) Jentzen, W.; Song, X.-Z.; Shelnutt, J. A. *J. Phys. Chem. B* **1997**, *101*, 1684.
(3) For a recent review of the possible biological significance of porphyrin nonplanar distortions see: Shelnutt, J. A.; Song, X.-Z.; Ma, J.-G.; Jia, S.-L.; Jentzen, W.; Medforth, C. J. *Chem. Soc. Rev.* **1998**, *27*, 31.

10.1021/ic010958a CCC: $25.00
Published on Web 03/06/2003

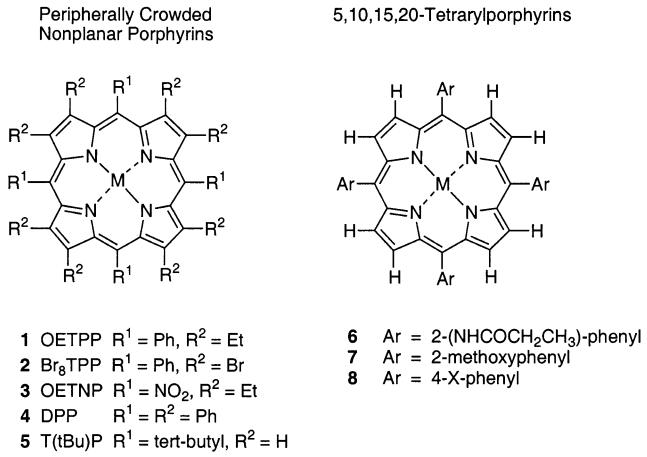

Figure 1. Structures of previously investigated peripherally crowded porphyrins and 5,10,15,20-tetraarylporphyrins.

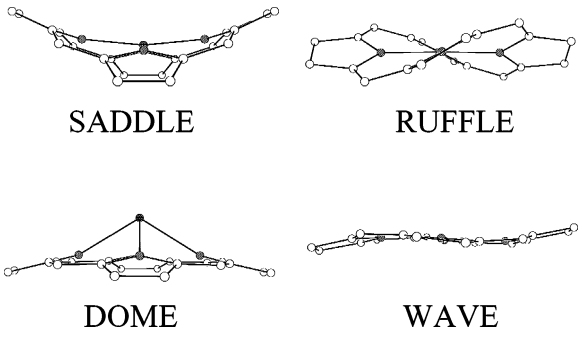

Figure 2. Representations of the lowest energy nonplanar distortion modes of the porphyrin macrocycle.[2]

produce materials such as molecular receptors[5−7] and molecular switches.[8]

Even though the effects of nonplanarity or peripheral crowding on the dynamic properties of porphyrins and other tetrapyroles might also be significant, to date this area has received comparatively little attention.[8−16] Optical studies have indicated that interconversion between different nonplanar conformations is likely a key factor determining the excited state dynamics of peripherally crowded porphyrins.[8−13] Variable temperature (VT) ^{1}H NMR investigations have shown that the activation energy for NH tautomerism is decreased in the strongly ruffled porphyrin H_2T(tBu)P (**5**, M = 2H),[14] and that the activation energies for axial ligand rotation are increased in cobalt(III) complexes of strongly ruffled T(tBu)P (**5**) or strongly saddled OETPP (**1**).[15,16] The decreased activation energy for NH tautomerism in H_2T(tBu)P has been rationalized[14] in terms of a contraction of the porphyrin core due to ruffling of the porphyrin macrocycle; this results in enhanced intramolecular hydrogen bonding of the NH protons, a situation which is analogous to the transition state for NH tautomerism. The higher barriers for ligand rotation were explained[15,16] by the ligands being oriented in deep cavities formed by the nonplanar porphyrin macrocycles and their substituents.

Table 1. Activation Energies for Aryl−Porphyrin Rotation ($\Delta G^{\ddagger}_{ROT}$; kJ mol^{-1}) in 5,10,15,20-Tetraarylporphyrins (TArPs)

porphyrin	M	$\Delta G^{\ddagger}_{ROT}$
6[19]	Zn^{II}	131
	Pd^{II}	130
	Cu^{II}	124
	Ni^{II}	108
	2H	122
	$4H^{2+}$	110
7[18]	2H	108
	$4H^{2+}$	96
8[17]	Ru^{II}(CO)(tBu-Py)	72−77[a]
	In^{III}Cl	63−71[a]
	Ti^{IV}=O	60−68[a]

[a] Depending upon the *para* substituent X.

Other changes in the dynamic properties of peripherally crowded nonplanar porphyrins versus regular porphyrins can reasonably be anticipated, and in this regard, it is interesting to note that differences between the activation energies for aryl−porphyrin rotation ($\Delta G^{\ddagger}_{ROT}$) in 5,10,15,20-tetraarylporphyrins (TArPs) such as **6**−**8** (Figure 1, Table 1) have long been thought to arise in significant part from nonplanar distortions and changes in the deformability of the macrocycle induced by the core substituent M.[17−19] For example, it has been hypothesized that ruffling induced by small metal ions (e.g., M = Ni^{II} vs Zn^{II} for porphyrin **6** or metals with higher oxidation states for porphyrin **8**) acts to move the *meso* aryl groups out-of-plane, thereby allowing them to rotate more easily and lowering $\Delta G^{\ddagger}_{ROT}$.[17,19] Nonplanarity has also been invoked to explain part of the observed decrease in $\Delta G^{\ddagger}_{ROT}$ for dications (M = $4H^{2+}$) compared to free base porphyrins (M = 2H) for **6** and **7**,[18,19] as protonation

(4) Recent investigations of the large red shifts seen in the optical spectra of peripherally crowded nonplanar porphyrins have led some research groups (Wertsching, A. K.; Koch, A. S.; DiMagno, S. G. *J. Am. Chem. Soc.* **2001**, *123*, 3932. Ryeng, H.; Ghosh, A. *J. Am. Chem. Soc.* **2002**, *124*, 8099) to propose that the observed shifts (and by implication the changes seen in other properties) are simply the result of substituent effects. A recent paper by our group (ref 73) confirms that the large red-shifts seen in peripherally crowded nonplanar porphyrins are indeed caused by nonplanar deformation and shows that the attribution of the red-shifts to substituent effects resulted from the use of inappropriate model structures in the earlier calculations.
(5) Mazzanti, M.; Marchon, J.-C.; Shang, M.; Scheidt, W. R.; Jia, S.; Shelnutt, J. A. *J. Am. Chem. Soc.* **1997**, *119*, 12400.
(6) Furusho, Y.; Kimura, T.; Mizuno, Y.; Aida, T. *J. Am. Chem. Soc.* **1997**, *119*, 5267.
(7) Muzzi, C. M.; Medforth, C. J.; Smith, K. M.; Jia, S.-L.; Shelnutt, J. A. *Chem. Commun.* **2000**, 131.
(8) Drain, C. M.; Gentemann, S.; Roberts, J. A.; Nelson, N. Y.; Medforth, C. J.; Jia, S. L.; Simpson, M. C.; Smith, K. M.; Fajer, J.; Shelnutt, J. A.; Holten, D. *J. Am. Chem. Soc.* **1998**, *120*, 3781.
(9) Gentemann, S.; Medforth, C. J.; Ema, T.; Nelson, N. Y.; Smith, K. M.; Fajer, J.; Holten, D. *Chem. Phys. Lett.* **1995**, *245*, 441.
(10) Drain, C. M.; Kirmaier, C.; Medforth, C. J.; Nurco, D. J.; Smith, K. M.; Holten, D. *J. Phys. Chem.* **1996**, *100*, 11984.
(11) Gentemann, S.; Nelson, N. Y.; Jaquinod, L.; Nurco, D. J.; Leung, S. H.; Medforth, C. J.; Smith, K. M.; Fajer, J.; Holten, D. *J. Phys. Chem. B* **1997**, *101*, 1247.
(12) Retsek, J. L.; Gentemann, S.; Medforth, C. J.; Smith, K. M.; Chirvony, V. S.; Fajer, J.; Holten, D. *J. Phys. Chem. B* **2000**, *104*, 6690.
(13) Retsek, J. L.; Medforth, C. J.; Nurco, D. J.; Gentemann, S.; Chirvony, V. S.; Smith, K. M.; Holten, D. *J. Phys. Chem. B* **2001**, *105*, 6396.
(14) Somma, M. S.; Medforth, C. J.; Nelson, N. Y.; Olmstead, M. M.; Khoury, R. G.; Smith, K. M. *Chem. Commun.* **1999**, 1221.
(15) Medforth, C. J.; Muzzi, C. M.; Smith, K. M.; Abraham, R. J.; Hobbs, J. D.; Shelnutt, J. A. *J. Chem. Soc., Chem. Commun.* **1994**, 1843.
(16) Medforth, C. J.; Muzzi, C. M.; Shea, K. M.; Smith, K. M.; Abraham, R. J.; Jia, S.; Shelnutt, J. A. *J. Chem. Soc., Perkin Trans. 2* **1997**, 833.
(17) Eaton, S. S.; Eaton, G. R. *J. Am. Chem. Soc.* **1977**, *99*, 6594.
(18) Dirks, J. W.; Underwood, G.; Matheson, J. C.; Gust, D. *J. Org. Chem.* **1979**, *44*, 2551.
(19) Freitag, R. A.; Whitten, D. G. *J. Phys. Chem.* **1983**, *87*, 3918.

typically distorts the porphyrin into a very saddled structure[1] to relieve crowding of the protons in the core. In the present work, we describe an investigation of the structures and aryl−porphyrin rotational barriers of some peripherally crowded and very nonplanar porphyrins based on the novel 2,3,5,7,8,10,12,13,15,17,18,20-dodecaphenylporphyrin (DPP) system **4**.

DPP and related 2,3,5,7,8,10,12,13,15,17,18,20-dodecaarylporphyrins (DArPs) have been widely studied during the past decade because of their unusual structural and spectroscopic properties.[10,12,13,20−37] Given the earlier studies of TArPs,[17−19] DArPs such as 5,10,15,20-tetraryl-2,3,7,8,-12,13,17,18-octaphenylporphyrins (TArOPPs; **10**) seemed to be ideal systems for further investigating the effect of nonplanar deformation on the aryl rotational barriers in porphyrins. The DArPs raise some interesting questions regarding the impact of nonplanar deformations on aryl−porphyrin rotational barriers. First, the dependence of the rotational barriers in the DArPs as a function of the core substituent M is not immediately obvious given that all of the complexes will be very nonplanar.[26,30,32] Second, although the addition of more aryl groups to the porphyrin macrocycle (e.g., eight phenyl groups to a TArP **9** to produce a TArOPP **10** or four phenyl groups to an OArP **11** to produce an OArTPP **13**) might be expected to significantly increase the peripheral steric crowding, and thus the rotational barriers, it is not clear to what extent the resulting nonplanar deformations will also attenuate the increase in rotational barrier. The aim of our study is to answer these and other related questions, and to see if it is possible to rationalize the aryl−porphyrin rotational barriers in DArPs using the same out-of-plane deformation model previously applied to TArPs.[17−19]

(20) Medforth, C. J.; Smith, K. M. *Tetrahedron Lett.* **1990**, *31*, 5583.
(21) Tsuchiya, S. *Chem. Phys. Lett.* **1990**, *169*, 608.
(22) Takeda, J.; Ohya, T.; Sato, M. *Chem. Phys. Lett.* **1991**, *183*, 384.
(23) Tsuchiya, S. *J. Chem. Soc., Chem. Commun.* **1991**, 716.
(24) Takeda, J.; Sato, M. *Inorg. Chem.* **1992**, *31*, 2877.
(25) Tsuchiya, S. J. *J. Chem. Soc., Chem. Commun.* **1992**, 1475.
(26) Medforth, C. J.; Senge, M. O.; Smith, K. M.; Sparks, L. D.; Shelnutt, J. A. *J. Am. Chem. Soc.* **1992**, *114*, 9859.
(27) Charlesworth, P.; Truscott, T. G.; Kessel, D.; Medforth, C. J.; Smith, K. M. *J. Chem. Soc., Faraday Trans.* **1994**, 1073.
(28) Takeda, J.; Sato, M. *Chem. Lett.* **1995**, 971.
(29) Takeda, J.; Sato, M. *Chem. Lett.* **1995**, 939.
(30) Nurco, D. J.; Medforth, C. J.; Forsyth, T. P.; Olmstead, M. M.; Smith, K. M. *J. Am. Chem. Soc.* **1996**, *118*, 10918.
(31) Clement, T. E.; Nguyen, L. T.; Khoury, R. G.; Nurco, D. J.; Smith, K. M. *Heterocycles* **1997**, *45*, 651.
(32) Barkigia, K. M.; Nurco, D. J.; Renner, M. W.; Melamed, D.; Smith, K. M.; Fajer, J. *J. Phys. Chem. B* **1998**, *102*, 322.
(33) Guilard, R.; Perie, K.; Barbe, J.-M.; Nurco, D.; Smith, K. M.; Van Caemelbecke, E.; Kadish, K. M. *Inorg. Chem.* **1998**, *37*, 973.
(34) Kadish, K. M.; Van Caemelbecke, E.; D'Souza, F.; Lin, M.; Nurco, D. J.; Medforth, C. J.; Forsyth, T. P.; Krattinger, B.; Smith, K. M.; Fukuzumi, S.; Nakanishi, I.; Shelnutt, J. A. *Inorg. Chem.* **1999**, *38*, 2188.
(35) Muzzi, C. M.; Medforth, C. J.; Voss, L.; Cancilla, M.; Lebrilla, C.; Ma, J.-G.; Shelnutt, J. A.; Smith, K. M. *Tetrahedron Lett.* **1999**, 6159.
(36) Kadish, K. M.; Lin, M.; Van Caemelbecke, E.; De Stefano, G.; Medforth, C. J.; Nurco, D. J.; Nelson, N. Y.; Krattinger, B.; Muzzi, C. M.; Jaquinod, L.; Xu, Y.; Shyr, D. C.; Smith, K. M.; Shelnutt, J. A. *Inorg. Chem.* **2002**, *41*, 6673.
(37) Retsek, J. L.; Drain, C. M.; Kirmaier, C.; Nurco, D. J.; Medforth, C. J.; Smith, K. M.; Chirvony, V. S.; Fajer, J.; Holten, D. Submitted for publication.

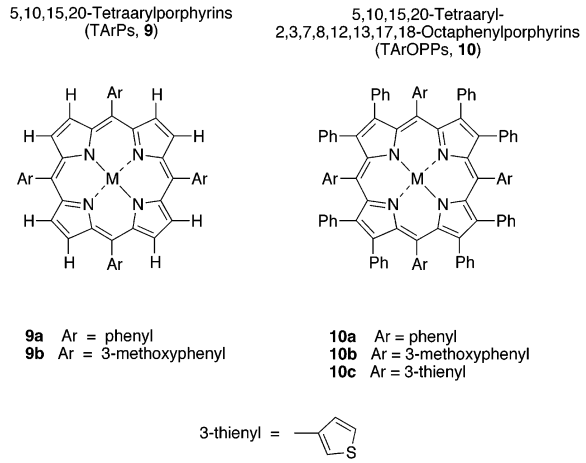

Figure 3. Structures of the investigated *meso* aryl-substituted porphyrins.

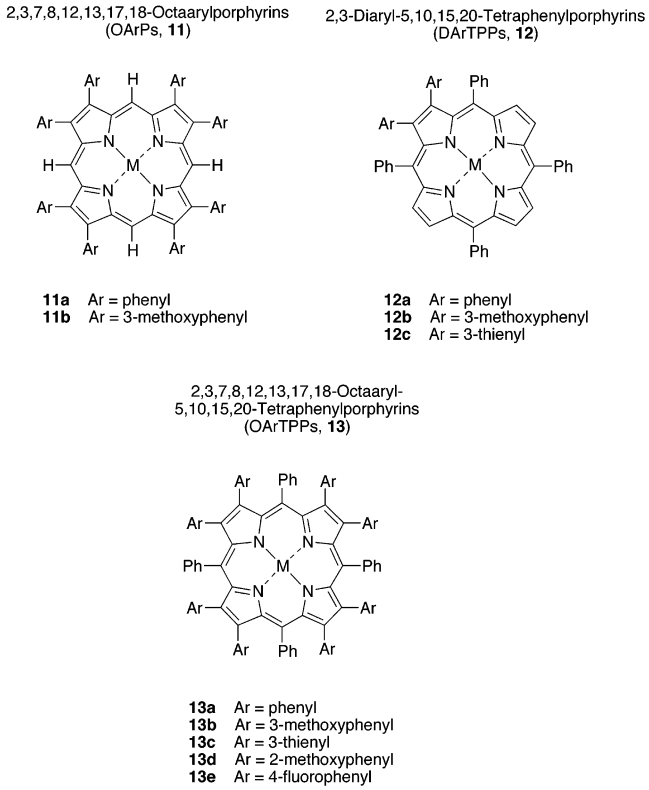

Figure 4. Structures of the investigated β aryl-substituted porphyrins.

The porphyrins investigated in our study can be divided into two general groups. The first group consists of the TArPs (**9**) and the highly substituted and very nonplanar 5,10,15,20-tetraryl-2,3,7,8,12,13,17,18-octaphenylporphyrins (TArOPPs; **10**) (Figure 3). These porphyrins were used to compare the barriers for rotation of *meso* aryl groups in uncrowded and crowded porphyrin systems, which is the primary focus of this study. The second group consists of the 2,3,7,8,12,13,17,18-octaarylporphyrins (OArPs; **11**) and the 2,3,7,8,12,13,17,18-octaaryl-5,10,15,20-tetraphenylporphyrins (OArTPPs; **13**) (Figure 4). These compounds were chosen to investigate the barriers for the rotation of β aryl groups in uncrowded and highly crowded porphyrins. In addition, the barriers for rotation of β aryl groups in an intermediately crowded system were investigated using some

2,3-diaryl-5,10,15,20-tetraphenylporphyrins (DiArTPPs; **12**). The core substituent effects examined in our study were chosen to match those previously studied for the TArPs.[17−19] The effect of metal size was investigated using complexes with a small metal (M = Ni) or a large metal (M = Zn). The effect of protonation was examined using the free base porphyrin (M = 2H) and the porphyrin dication (M = $4H^{2+}$).

As in the previous studies of TArPs,[17,18,38−41] variable temperature (VT) ^{1}H NMR spectroscopy is used to determine the aryl−porphyrin rotational barriers. In such experiments, it is usually necessary to generate asymmetry in the porphyrin complex, either by the use of asymmetrical aryl substituents[18,38,39,41] or by asymmetrical ligation of a centrally coordinated metal ion.[17,39,40] The former approach was employed in this study, and porphyrins **9b**, **10b**, **11b**, **12b**, and **13b**, where the aryl group is 3-methoxyphenyl, were synthesized. The 3-methoxyphenyl group was chosen as the standard substituent because it could be readily introduced onto the porphyrin macrocycle using existing synthetic methodologies.[35,42] As some of the porphyrins used in our studies are known to display additional dynamic processes such as NH tautomerism and macrocyclic inversion,[43] aryl substituents with varying steric requirements, and thus different rotational barriers, were used to unambiguously assign the aryl-porphyrin rotation process. The 2-methoxyphenyl group has been employed in earlier studies of 5,10,15,20-tetraarylporphyrins[18] and was also used in this study to increase the aryl−porphyrin rotational barrier (porphyrin **13d**). The 3-thienyl substituent was successfully tested as a way to lower the aryl−porphyrin rotational barrier (porphyrins **10c**, **12c**, and **13c**).

In section I of the Results and Discussion section, X-ray crystallographic studies of the TArPs, OArPs, DArPs (TArOPPs/OArTPPs), and DiArTPPs are described. The crystal structures are then analyzed using normal-coordinate structural decomposition (NSD),[2] a recently developed technique for quantifying the out-of-plane deformations in porphyrins. In this way, the effects of different peripheral or core substituents on the conformation of the macrocycle are delineated. Note that the majority of the compounds discussed in this section contain symmetrical aryl substituents (mainly phenyl rings) and are thus not identical to the compounds used in the VT NMR studies or the molecular mechanics (MM) calculations (e.g., the X-ray data is based on structure **9a** rather than on structure **9b**). However, molecular mechanics calculations indicate that the effect of the methoxyl substituent on the macrocycle conformation is small.

In section II, MM calculations[44−46] are used to calculate the barriers for aryl−porphyrin rotation in TArP **9b** and TArOPP **10b**. MM calculations were carried out because the rotational barriers may be dependent on the ability of the porphyrin to deform along a particular coordinate during the rotation process, an effect that may not always be reflected in the crystallographic data. The MM calculations allow us to examine the conformational changes that occur for the porphyrin macrocycle during the aryl−porphyrin rotation process. Finally, in section III, the barriers for aryl−porphyrin rotation are determined experimentally using variable temperature (VT) ^{1}H NMR spectroscopy. The NMR results are then interpreted in terms of the available structural information and the barriers compared to the results obtained from the MM calculations.

Results and Discussion

I. X-ray Crystallographic Studies. In this section, X-ray crystallography is used to investigate the relationship between the peripheral and core substituents present for the TArPs, OArPs, DArPs (TArOPPs/OArTPPs), or DiArTPPs and the conformation of the porphyrin macrocycle. Particular emphasis is placed on determining the conformations of the DArPs and comparing them to those seen for the TArPs. Note that the compounds investigated in this section are not necessarily identical to those discussed in sections II and III. This is because the compounds used in the NMR studies in section III have asymmetrical aryl substituents to allow rotation to be detected, whereas most of the porphyrins examined by X-ray crystallography have phenyl substituents or symmetrical aryl substituents to avoid the problems presented by the porphyrin crystallizing with multiple orientations of the aryl substituents (atropisomers). The effect on the structure of adding or changing a substituent (e.g., adding a methoxyl group at the *meta* position of the phenyl ring) is expected to be small in the systems we are studying, as confirmed by the MM calculations discussed in section II, so it will not alter the conclusions reached in our work.

Full details of the synthesis, characterization, and crystal structure determinations of the porphyrins investigated in our study are provided in the Experimental Section. Table 2 provides crystallographic data for the new crystal structures reported in this paper. Tables 3 and 4 summarize the nonplanar deformations for the TArPs, OArPs, DArPs, and DiArTPPs as determined using normal-coordinate structural decomposition (NSD).[2,46] NSD is a recently developed procedure for quantitatively analyzing the out-of-plane (and in-plane) deformations of porphyrins. The NSD method characterizes the porphyrin conformation in terms of equivalent displacements (normal deformations) along the normal coordinates of the D_{4h}-symmetric porphyrin macrocycle. Nonbonded interactions at the porphyrin periphery obtained from selected X-ray structures, which are used as an

(38) Walker, F. A.; Avery, G. L. *Tetrahedron Lett.* **1971**, *52*, 4949.
(39) Eaton, S. S.; Eaton, G. R. *J. Chem. Soc., Chem. Commun.* **1974**, 576.
(40) Eaton, S. S.; Eaton, G. R. *J. Am. Chem. Soc.* **1975**, *97*, 3660.
(41) Crossley, M. J.; Field, L. D.; Forster, A. J.; Harding, M. M.; Sternhell, S. *J. Am. Chem. Soc.* **1987**, *109*, 341.
(42) Takeda, J.; Sato, M. *Chem. Pharm. Bull.* **1994**, *42*, 1005.
(43) For a recent review of NMR spectroscopy of diamagnetic porphyrins see: Medforth, C. J. In *The Porphyrin Handbook*; Kadish, K. M., Smith, K. M., Guilard, R., Eds.; Academic Press: Boston, 2000; Vol. 5; p 1.
(44) Shelnutt, J. A.; Medforth, C. J.; Berber, M. D.; Barkigia, K. M.; Smith, K. M. *J. Am. Chem. Soc.* **1991**, *113*, 4077.
(45) Song, X.-Z.; Jaquinod, L.; Jentzen, W.; Nurco, D. J.; Jia, S.-L.; Khoury, R.; Ma, J.-G.; Medforth, C. J.; Smith, K. M.; Shelnutt, J. A. *Inorg. Chem.* **1998**, *37*, 2009.
(46) For a recent review see: Shelnutt, J. A. In *The Porphyrin Handbook*; Kadish, K. M., Smith, K. M., Guilard, R., Eds.; Academic Press: Boston, 2000; Vol. 7; p 167.

Table 2. Crystallographic Data for **12c** (M = Ni), **13c** (M = Ni), and **13e** (M = $4H^{2+}$)

	12c (M = Ni)	**13c** (M = Ni)	**13e** (M = $4H^{2+}$)
chemical formula	$C_{52}H_{26}N_4Ni_1S_2$	$C_{76}H_{44}N_4NiS_8$ ·2.6($CHCl_3$)	$C_{92}H_{56}F_8N_4^{2+}$ ·2($C_6H_2N_3O_7$)$^-$ ·4.5(CH_2Cl_2)
fw	835.68	1638.80	2207.79
space group	*C*2/*c* (No. 15)	$I4_1/a$ (No. 88)	$P2_1/c$ (No. 14)
a (Å)	24.2800(10)	23.192(2)	14.7084(5)
b (Å)	15.3387(6)	23.192(2)	24.5060(8)
c (Å)	10.7881(4)	82.412(7)	29.1288(10)
β (deg)	105.808(1)	90	103.130(1)
V (Å^3)	3865.8(3)	44328(5)	10224.8(6)
Z	4	24	4
λ (Å)	0.71073	1.54178	0.71073
T (K)	90(2)	130(2)	90(2)
μ (mm^{-1})	0.655	5.314	0.344
D_{calcd} (g cm^{-3})	1.434	1.454	1.452
R1 (F_o^2) (>2σ(*I*))[a]	0.0550	0.1256	0.1015
wR2 (F_o^2) (all data)[a]	0.1572	0.3495	0.3421

[a] R1 = $\sum||F_o - F_c||/\sum|F_o|$ and wR2 = $[\sum[w(F_o^2 - F_c^2)^2]/\sum[w(F_o^2)^2]]^{1/2}$, $w = 1/[\sigma^2(F_o^2) + ((X)P)^2 + (Y)P]$ where $P = (F_o^2 + 2F_c^2)/3$. For **12c** (M = Ni): $X = 0.0876000$ and $Y = 5.91870$. For **13c** (M = Ni): $X = 0.173300$ and $Y = 1304.26$. For **13e** (M = $4H^{2+}$): $X = 0.198600$ and $Y = 17.7353$.

approximate measure of the steric crowding of the aryl substituents, are presented in Table 5.

We consider first the published data for the uncrowded TArP parent system 5,10,15,20-tetraphenylporphyrin (TPP, **9a**) and the uncrowded OArP parent system 2,3,7,8,12,13,17,18-octaphenylporphyrin (OPP, **11a**). Table 3 lists the total out-of-plane deformation (d_{obsd}) calculated using all the out-of-plane modes, as well as the contributions from the lowest frequency mode of each symmetry type (e.g. d_{sad} which corresponds to the lowest energy B_{2u} 'saddling' mode).[47] These low frequency modes typically encompass most of the nonplanar deformation.[2] The saddling (sad), ruffling (ruf), doming (dom), and waving (wav) modes discussed in Table 3 are those illustrated in Figure 2.

The ruffling (ruf) and saddling (sad) distortions constitute the majority of the nonplanar deformation observed in each structure (Table 3) with smaller contributions from the doming (dom), waving (wav), and propellering (pro) modes. This is not surprising as ruffling and saddling are the softest out-of-plane modes and therefore produce the largest out-of-plane distortions.[2] The following discussion is restricted to the energetically relevant ruf and sad deformation modes, which conveniently correspond to out-of-plane displacements along the axes of substitution for the porphyrins investigated in our study. For example, ruffling will move the *meso* aryl substituents out-of-plane whereas saddling will move the β aryl substituents out-of-plane (see Figure 2).

TPP is the most extensively investigated of all the aryl-substituted porphyrins, and crystal structures have been reported for the zinc complex (ZnTPP), the nickel complex (NiTPP), the free base porphyrin (H_2TPP), and the dication (H_4TPP^{2+}). The crystallographic studies show that ZnTPP is essentially planar (d_{obsd} 0.2−0.3 Å), NiTPP is slightly ruffled (d_{ruf} 1.3 Å), H_2TPP is typically planar (although a slightly ruffled structure has been reported), and H_4TPP^{2+} is strongly saddled irrespective of the anion present (d_{sad} 2.5−3.3 Å). No structural data is available for OPP, possibly because of the low solubility of this compound.[48] However, it is likely to be very similar to that of 2,3,7,8,12,13,17,18-octaethylporphyrin (OEP) for which numerous crystal structures have been reported including ZnOEP, NiOEP, H_2OEP, and H_4OEP^{2+} (Table 3). Overall, the structural trends seen for OEP as a function of the core substituent M are similar to those seen for TPP, although OEP seems to be more flexible and more planar than TPP. This is evidenced by NiOEP crystallizing in planar or ruffled conformations, and by the amount of distortion seen for H_4OEP^{2+} being strongly dependent upon the anion.

The structural changes seen for OEP and TPP as a function of M are also seen for other porphyrins.[1,49] Generally, small metals which require short metal−nitrogen distances favor ruffling because this distortion mode produces the smallest core.[45] In contrast, protonation favors saddling because this deformation reduces the steric crowding between the protons in the core. The earlier interpretations[17−19] of the rotational barriers in TArPs were based in large part on the X-ray for TPP and OEP. The ruffling apparent for the nickel complexes but not for the zinc complexes was used to explain the lower rotational barrier in **6** (M = Ni) versus **6** (M = Zn)[19] (Table 1). It was suggested that the easier deformation and concomitant out-of-plane movement of the aryl groups in the nickel complexes of TArPs facilitated aryl−porphyrin rotation by relieving interactions between the aryl group and the porphyrin macrocycle.[17,19] Nonplanar deformation (saddling) was also invoked to explain the lower barriers in the dications versus the free bases of porphyrins **6** and **7**.[18,19]

In an earlier report,[19] it was suggested that the nonplanar distortions seen in the crystal structures of nickel porphyrins might be viewed as the "limit of deformability", with the zinc atom enforcing a planar structure and restricting deformation. Curiously, an analysis of the close contacts at the porphyrin periphery for ruf NiTPP and planar ZnTPP shows that the distance between the *ipso* carbons of the *meso* phenyl rings and the β pyrrole carbons are similar (2.92 Å). This makes it difficult to understand the decrease in rotational barrier purely on the basis of the static distortions seen in the crystal structures and suggests that the nickel complex deforms more during the rotation process than is apparent in the X-ray structure (i.e., the deformability of the macrocycle is important).

The TArP dications are expected to be difficult to deform by ruffling because the resulting strong contraction of the core[45] will significantly increase steric interactions between the four inner hydrogens. A more probable mechanism for lowering the rotational barriers in the TArP dications would seem to be an increase in the conformational space available to the *meso* aryl substituent due to the large out-of-plane movement of the adjacent pyrrole rings upon saddling. In

(47) Note that d_{obsd} is calculated as the square root of the sum of the squares for all the modes.

(48) Takeda, J.; Ohya, T.; Sato, M. *Chem. Pharm. Bull.* **1990**, *38*, 264.
(49) Sparks, L. D.; Medforth, C. J.; Park, M.-S.; Chamberlain, J. R.; Ondrias, M. R.; Senge, M. O.; Smith, K. M.; Shelnutt, J. A. *J. Am. Chem. Soc.* **1993**, *115*, 581.

Table 3. NSD Analysis of the Out-of-Plane Deformations for TPP and OEP Complexes

porphyrin	CCDC refcode	d_{obsd}[a]	d_{sad} (B_{2u})[b]	d_{ruf} (B_{1u})	d_{dom} (A_{2u})	$d_{wav(x)}$ ($E_{g(x)}$)	$d_{wav(y)}$ ($E_{g(y)}$)	d_{pro} (A_{1u})
ZnTPP (monoclinic)	ZZZTAY03	0.175	0.000	0.000	0.000	−0.158	0.018	0.000
ZnTPP (triclinic)	ZZZTAY02	0.297	0.000	0.000	0.000	−0.194	0.136	0.000
NiTPP	ZZZUUC01	1.295	−0.256	−1.266	0.000	0.000	0.000	−0.001
H_2TPP	TPHPOR01	0.333	0.000	0.000	0.000	0.114	0.232	0.000
H_2TPP [benzyl alcohol]	JIVRAH	0.046	0.000	0.000	0.000	0.009	0.011	0.000
H_2TPP [*m*-xylene]	SEMNIH	0.065	0.000	0.000	0.000	0.003	0.039	0.000
H_2TPP [*p*-xylene]	SEMNUT	0.233	0.000	0.000	0.000	0.057	0.197	0.000
H_2TPP	TPHPOR10	1.082	0.183	1.055	0.000	0.000	0.000	0.000
$H_4TPP^{2+}(HSO_4)_2$	LEXSIQ	2.520	2.434	0.000	0.045	0.000	0.031	0.000
$H_4TPP^{2+}(CF_3CO_2)_4(UO_2)$	CAXHAK	2.670	2.586	0.169	0.025	0.000	0.068	0.022
$H_4TPP^{2+}(ClO_4)_2$ [C_6H_6]	RUHQEQ	2.743	2.662	0.000	0.181	0.053	0.108	0.014
$H_4TPP^{2+}(ClO_4)_2$ [CH_3OH]	YEVJAN	3.042	2.964	0.007	0.021	0.069	0.040	0.024
$H_4TPP^{2+}(Cl)(FeCl_4)$	TPPFEC	3.272	3.114	0.754	0.000	0.000	0.000	0.000
ZnOEP(1-Me-Im)	GAKWEU	0.273	0.082	0.041	0.236	0.040	0.012	−0.010
ZnOEP(Py)	EPOPZN10	0.330	−0.098	0.026	−0.278	0.137	−0.009	0.005
NiOEP (tetragonal)	NOEPOR	1.461	−0.116	1.456	0.000	0.000	0.000	0.000
NiOEP (triclinic A)	NOEPOR11	0.087	0.000	0.000	0.000	0.072	−0.031	0.000
NiOEP (triclinic B)	NOEPOR02	0.144	0.000	0.000	0.000	−0.066	−0.117	0.000
H_2OEP	OETPOR10	0.126	0.000	0.000	0.000	0.063	0.090	0.000
$H_4OEP^{2+}Rh(CO)_2Cl_2$	HOETPN	0.085	0.000	0.000	0.000	0.060	0.006	0.000
$H_4OEP^{2+}(CH_3SO_4)_2$	LEYFOK	1.221	1.113	0.186	0.082	0.064	0.097	0.044
$H_4OEP^{2+}(ClO_4)_2$	RUHQAM	1.389	1.276	0.346	0.036	0.005	0.123	0.060
$H_4OEP^{2+}(CF_3CO_2)_2$	YEVKIT	2.137	2.056	0.210	0.101	0.018	0.109	0.006

[a] Total out-of-plane deformation (Å). [b] Deformation in the lowest frequency mode of each symmetry type (Å).

Table 4. NSD Analysis of the Out-of-Plane Deformations for DArP and DiArTPP Complexes

porphyrin	CCDC refcode	d_{obsd}[a]	d_{sad} (B_{2u})[b]	d_{ruf} (B_{1u})	d_{dom} (A_{2u})	$d_{wav(x)}$ ($E_{g(x)}$)	$d_{wav(y)}$ ($E_{g(y)}$)	d_{pro} (A_{1u})
H_2DiEtTPP	TATPOT01	0.619	−0.596	−0.055	0.044	0.031	−0.137	0.022
ZnDiEtTPP (3-picoline)	RUTNEZ	1.066	−0.896	−0.473	0.162	0.156	0.187	−0.010
ZnDiEtTPP (MeOH)	RUTNID	0.361	0.328	−0.035	−0.085	−0.086	0.042	−0.006
NiDiEtTPP	RUTMUO	2.648	−2.520	0.782	0.036	0.147	0.000	0.013
12c (M = Ni)	this work	0.131	0.000	−0.128	0.000	0.000	0.005	−0.001
Zn^{II} DPP #1	ZAWRES	2.896	−2.882	0.000	−0.084	0.000	0.000	0.000
Zn^{II} DPP #2	XAWSAP	3.074	3.059	0.000	0.000	0.000	0.000	0.000
Ni^{II} DPP #1	TEZXIF	2.441	−0.060	−2.439	0.000	0.000	0.000	0.000
Ni^{II} DPP #2	XAWROC	3.550	−3.098	−1.707	−0.156	0.000	0.000	−0.083
Ni^{II} DPP #3	XAWRUI	2.717	0.917	−2.555	0.051	−0.027	0.009	−0.028
Ni^{II} DPP #4	XAWSET	2.522	0.827	−2.377	0.058	0.004	−0.040	−0.014
13c (M = Ni) molecule 1	this work	3.282	−2.770	−1.751	0.002	−0.004	0.062	0.019
13c (M = Ni) molecule 2	this work	2.826	1.247	−2.530	−0.079	0.000	0.000	0.078
H_2DPP #1	LADGAY	3.032	2.963	0.000	0.499	−0.098	0.000	0.000
H_2DPP #2	XAWRIW	3.922	3.835	0.000	−0.173	−0.184	0.000	0.000
13e (M = $4H^{2+}$) $(picrate)_2$	this work	3.858	3.769	0.420	−0.016	−0.049	0.221	0.031

[a] Total out-of-plane deformation (Å). [b] Deformation in the lowest frequency mode of each symmetry type (Å).

Table 5. Nonbonded Interactions (Å) at the Periphery of the Aryl-Substituted Porphyrins

porphyrin	CCDC refcode	conformation	C_{ipso}(*meso*), C(β)	C_{ipso}(*meso*), C_{ipso} (β)	C_{ipso} (β), C_{ipso} (β)′	C_{ipso} (β), C(*meso*)
ZnTPP (monoclinic)	ZZZTAY03	planar	2.92	N/A	N/A	N/A
NiTPP	ZZZUUC01	ruffled	2.92	N/A	N/A	N/A
H_2TPP	SEMNIH	planar	2.91	N/A	N/A	N/A
H_4TPP^{2+} $(ClO_4)_2$ [CH_3OH]	YEVJAN	saddled	3.04	N/A	N/A	N/A
Zn^{II} DPP #1	ZAWRES	saddled	3.01	3.02	3.06	3.25
Ni^{II} DPP #1	TEZXIF	ruffled	3.01	3.00	2.95	3.26
H_2DPP #1	LADGAY	saddled	3.03	3.04	3.13	3.21
13e (M = $4H^{2+}$) $(picrate)_2$	this work	saddled	3.10	3.12	3.16	3.20

this regard, it is worth noting that saddling in the TArP dications can result in a displacement out of the porphyrin least-squares plane of greater than 1 Å for the pyrrole β carbon atoms. An examination of the close contacts shows that in the case of protonation there is indeed a significant increase in the C_{ipso}(*meso*)−Cβ distance (from 2.91 to 3.04 Å). This may indicate a mechanistic dichotomy in how core substituents lower the aryl−porphyrin rotational barriers in TArPs. Small metals might favor out-of-plane rotation due to their greater deformability via ruffling, whereas protonation might favor in-plane rotation due to the increased conformational space achieved by saddling the macrocycle. We will return to this point in the molecular mechanics calculations described in section II.

We now turn to the peripherally crowded and very nonplanar dodecaarylporphyrins (DArPs). 2,3,5,7,8,10,12,-13,15,17,18,20-Dodecaphenylporphyrin (DPP, **4**) is the parent DArP from which TArOPPs **10** and OArTPPs **13** are

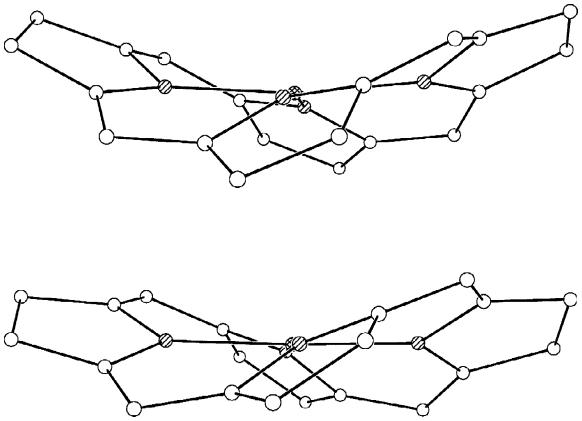

Figure 5. The two independent molecules seen in the crystal structure of **13c** (M = Ni). The aryl substituents have been omitted to better illustrate the conformations of the porphyrin macrocycles.

derived. DPP has been the subject of several crystallographic investigations,[26,30,32] all of which have shown that the porphyrin macrocycle is very distorted due to the need to minimize steric repulsions between the peripheral phenyl substituents. The two crystal structures reported for ZnDPP[32] show quite similar amounts of nonplanar deformation (d_{obsd} approximately 3 Å) that is predominantly of the sad type (Table 4). The two crystal structures reported for H_2DPP[26,32] also show primarily sad distortion of the porphyrin macrocycle, although a significant doming component is present for the first structure (LADGAY). The second structure (XAWRIW) is significantly more nonplanar than the first (d_{obsd} 3.9 vs 3.0 Å). No fewer than four X-ray structures have been reported for NiDPP.[30,32] These show that the macrocycle can adopt structures with ruf and/or sad deformations; i.e., the macrocycle is conformationally flexible with this metal. One structure (CCDC refcode TEZXIF) is ruf, two (XAWUI and XAWSET) are mainly ruf with some sad deformation, and one (XAWROC) is sad with a significant amount of ruf deformation. The increased preference of the nickel complex versus the zinc complex for a ruffled conformation has an obvious structural rationale given the known tendency of nickel to favor short metal−nitrogen distances and the greater core contraction that occurs with ruf versus sad deformation.[45]

The greater conformational flexibility of the nickel complexes of the DArPs was also seen in the present study in the crystal structure of OArTPP **13c** (M = Ni), one of the porphyrins used in the NMR experiments in section III. Porphyrin **13c** (M = Ni) is not an ideal candidate for a crystal structure determination because of the many different isomers (atropisomers) possible for this molecule. However, it did yield crystals suitable for a structure determination, and the resulting structure is shown in Figure 5. As expected, the 3-thienyl groups are rotationally disordered over two positions. More significantly, porphyrin **13c** (M = Ni) adopts two different conformations in the asymmetric unit (Figure 5). Both conformations are very nonplanar (d_{obsd} = 3.3 and 2.8 Å) and contain mixtures of sad and ruf deformations. Conformation 1 has principally sad deformation, and conformation 2 has mainly ruf deformation (Table 4). The Ni−N bond distances in **13c** (M = Ni) are short (1.896 Å in conformation 1 and 1.878 Å in conformation 2) as described for other very nonplanar porphyrins [e.g., 1.885−1.909 Å in NiDPP and 1.906 Å in NiOETPP (**1**, M = Ni)].[50] Note that this is not the first time that two independent molecules have been found in the asymmetric cell of a peripherally crowded porphyrin. A similar phenomenon has been reported for NiOETNP (**3**, M = Ni).[51]

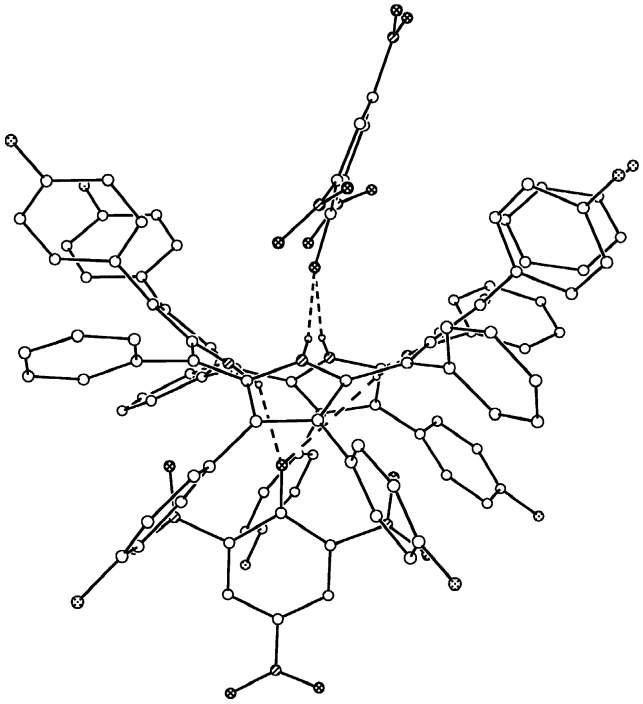

Figure 6. Crystal structure of **13e** (M = $4H^{2+}$) $(pic)_2$. Hydrogen atoms, except for those in the core, have been omitted for clarity. Hydrogen-bonding interactions are indicated by dashed lines.

Crystallographic data has not been reported for the dication of dodecaphenylporphyrin (H_4DPP^{2+}) or any other DArP (TArOPP or OArTPP), but such a structure was required to complete our series of porphyrins with different core substituents. Attempts to grow crystals of H_4DPP^{2+} suitable for X-ray crystallographic studies were unsuccessful using a range of acids (trifluoroacetic, hydrochloric, and picric acids) with several crystallization techniques. However, we were able to grow crystals of OArTPP **13e** (M = $4H^{2+}$), which has 4-fluorophenyl rather than phenyl groups at the β position of the porphyrin (see Figure 4), using picric acid. The presence of a fluoro group at the para positions of the β phenyl rings is expected to have a minimal impact on the observed structure.

As far as we are aware, this is the first time that the structure of the picrate salt of a porphyrin dication has been determined. The structure of porphyrin **13e** (M = $4H^{2+}$) $(pic)_2$ displays a very nonplanar conformation (Figure 6). The nonplanar deformation (d_{obsd} 3.9 Å) is predominantly sad (3.8 Å) with a small amount of ruf (0.4 Å).[47] The tilt angle of a pyrrole ring with respect to the least-squares plane

(50) Barkigia, K. M.; Renner, M. W.; Furenlid, L. R.; Medforth, C. J.; Smith, K. M.; Fajer, J. *J. Am. Chem. Soc.* **1993**, *115*, 3627.
(51) Senge, M. O. *J. Chem. Soc., Dalton Trans.* **1993**, 3539.

of the porphyrin macrocycle is as large as 41°. The nonplanarity of the structure is greater than seen in the first crystalline modification of H_2DPP (d_{obsd} 3.0 Å) and in the dications of TPP (d_{obsd} 2.5−3.3 Å) or OEP (d_{obsd} 0.1−2.1 Å) but is comparable to that seen in the second crystalline form of H_2DPP (d_{obsd} 3.9). Overall, the structure of **13e** (M = $4H^{2+}$) $(pic)_2$ is consistent with the known tendency of both peripheral crowding and protonation to increase nonplanarity of the porphyrin macrocycle (i.e., it is more nonplanar than the less crowded H_4TPP^{2+} and than at least one form of unprotonated H_2DPP).

Hydrogen atoms were observed on each of the pyrrole nitrogen atoms indicating that two protons were donated by the picric acid molecules to the porphyrin macrocycle. Compound **13e** (M = $4H^{2+}$) $(pic)_2$ should therefore be classified as a salt and not as a complex.[52] The picrate anions are oriented approximately parallel to the cavities formed on either side of the macrocycle by the saddling of the porphyrin ring and the 4-fluorophenyl substituents on the pyrrole rings. A similar orientation effect has been observed for the aromatic amine ligands in cobalt(III),[15,16] nickel,[53] and iron[54] complexes of OETPP. A significant difference between the picrate anions and the aromatic amine ligands is the tilting of the aromatic plane away from the perpendicular for the picrates (Figure 6).

The picrate anion on the upper face of the molecule is disordered over both tilting positions, although only the right tilting position is shown in Figure 6. The distances between the porphyrin nitrogen atoms and the picrate phenolate oxygen atom for the upper picrate are 2.90 Å (N3−O8) and 3.04 Å (N1−O8). These are longer than the corresponding N−O(phenolate) distances in pyridinium picrate (2.62 Å)[55] and imidazolium picrate (2.71 and 2.83 Å)[56] but comparable to the N−O distances in the perchlorate salts of TPP (CCDC refcode RUHQEQ) and OEP (RUHQAM) (2.99 and 2.95 Å). The lower picrate anion is not disordered but is slipped along the cavity (to the left in Figure 6). This results in considerable asymmetry in the N−O(phenolate) distances (2.74 Å for N2−O1 and 3.88 Å for N4−O). The slippage may be possible because N4 can also interact with one of the oxygen atoms (O7) from a nitro group (N−O distance 2.88 Å). A related interaction between the pyridinium nitrogen and the oxygen atom of one of the picrate nitro groups has been observed in pyridinium picrate (N−O distance 2.92 Å).[55]

In summary, the structural data for the DPPs (DArPs) shows that a sad conformation is favored by the macrocycle when M = Zn, 2H or $4H^{2+}$, but both the sad and/or the ruf conformations can be accessed when a small metal (Ni^{II}) is present. The ability of the Ni^{II} complexes to access the ruf conformation is presumably the result of the ruf conformation being better able to provide the short metal−nitrogen distance favored by Ni^{II}. Overall, the structural changes seen for the DArPs as a function of the core substituent M are similar to those seen for the TArPs: switching to a smaller metal (Ni vs Zn) increases the tendency of the macrocycle to ruffle, whereas protonation increases the amount of saddle deformation (at least compared to one H_2DPP structure).

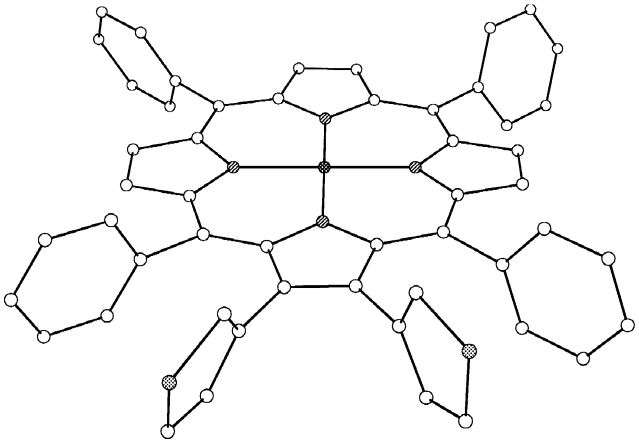

Figure 7. Crystal structure of porphyrin **12c** (M = Ni). Hydrogen atoms have been omitted for clarity, and only one orientation of the rotationally disordered 3-thienyl rings is shown.

The close contacts at the periphery of the macrocycle for the DArPs are given in Table 5. The trends in the close contacts for the *meso* aryl substituents in the DArPs parallel those seen for the TArPs but are about 0.1 Å longer in the case of the DArPs. The C_{ipso}(*meso*)−Cβ distances are about the same (3.02 ± 0.01 Å) for ruf NiDPP, sad ZnDPP, and H_2DPP (CCDC refcode LADGAY) but approximately 0.1 Å greater for **13e** (M = $4H^{2+}$) $(pic)_2$. A similar pattern is seen for the distance between C_{ipso}(*meso*) and C_{ipso}(β). Based purely on these findings, it would seem reasonable to expect the dication to have the lowest aryl−porphyrin rotational barrier, although as we will show later this is not the case.

Finally, we examined DiArTPPs **12** which are of intermediate peripheral crowding. By analogy with previous studies of the effects of peripheral substitution,[1] the addition of two phenyl substituents to the β position of TPP (**9a**) to produce the intermediately crowded DiArTPP 2,3,5,10,15,-20-hexaphenylporphyrin (HPP, **12a**) might be expected to increase the amount of nonplanar deformation. Such an increase in nonplanar deformation compared to TPP has been observed in the related 2,3-diethyl-5,10,15,20-tetraphenylporphyrins (DiEtTPPs) reported by Senge and Kalisch[57] (Table 4). Interestingly, the crystal structure of DiArTPP **12c** (M = Ni) (Figure 7) shows that the macrocycle is not appreciably distorted. The molecule is approximately planar (d_{obsd} 0.13 Å, Table 4) and is actually less nonplanar than NiTPP (d_{obsd} 1.30 Å, Table 3). The mean deviation of an atom from the least-squares plane of the porphyrin ring for **12c** (M = Ni) is only 0.02 Å, and the angles between the pyrrole planes and the least-squares plane of the porphyrin ring are less than 2°. The average Ni−N distance (1.963 Å) is also quite

(52) Herbstein, F. H.; Moshe, K. *Acta Crystallogr.* **1991**, *C47*, 1131.
(53) Renner, M. W.; Barkigia, K. M.; Melamed, D.; Smith, K. M.; Fajer, J. *Inorg. Chem.* **1996**, *35*, 5120.
(54) Ogura, H.; Yatsunyk, L.; Medforth, C. J.; Smith, K. M.; Barkigia, K. M.; Renner, M. W.; Melamed, D.; Walker, F. A. *J. Am. Chem. Soc.* **2001**, *123*, 6564.
(55) Takayanagi, H.; Kawaoka, R.; Chin, K.; Goto, M.; Yamaguchi, S.-I.; Ogura, H. *Anal. Sci.* **1990**, *6*, 321.
(56) Soriano-Garcia, M.; Schatz-Levine, M.; Toscano, R. A.; Villena Iribe, R. *Acta Crystallogr.* **1990**, *C46*, 1556.
(57) Senge, M. O.; Kalisch, W. W. *Inorg. Chem.* **1997**, *36*, 6103.

long and consistent with those seen in other planar nickel porphyrins (e.g., triclinic A NiOEP 1.958 Å).[58] The macrocycle does show a slight elongation along the axis of the substituted pyrrole ring leading to longer average Ni−N distances in this direction (1.982 vs 1.945 Å). However, the additional aryl rings at the pyrrole position of **12c** (M = Ni) appear to do little to increase the amount of nonplanar distortion.

The finding that **12c** (M = Ni) is more substituted but also more planar than NiTPP underscores the need for caution when interpreting the spectroscopic properties of porphyrins using the static picture obtained from X-ray crystallographic studies. The apparently anomalous behavior of **12c** (M = Ni) is probably related to the fact that the energy required to deform the macrocycle is small for small amounts of deformation; i.e., there is a fairly shallow potential energy surface.[59] This is particularly true for porphyrins with small metals such as nickel, where there is a tradeoff between the structural requirements of the metal (short metal−nitrogen distance, which favors ruffling) and the porphyrin ring (maximizing π-overlap, which favors a planar macrocycle). Given the fine balance between these two forces, the crystallization conditions and crystal packing forces become important in determining the observed conformation. For example, it is known that NiOEP exists in both planar and nonplanar conformations in the solid state (Table 3) and in solution.[60,61] It is probable that **12c** (M = Ni) exhibits similar behavior.

II. Molecular Mechanics (MM) Calculations. Molecular simulations are increasingly being used to investigate the structural and dynamic properties of porphyrins.[46] We decided to determine if molecular mechanics (MM) calculations might provide additional insights into the structural preferences of the TArPs and DArPs as well as the aryl−porphyrin rotation processes in these systems. MM calculations were carried out using POLYGRAF software (Molecular Simulations, Inc.) and a force field for metalloporphyrins that has been used extensively to calculate the structures of porphyrins[7,8,26,44−46,49,62−73] and to investigate some dynamic processes (e.g., axial ligand rotation).[15,16] The modified DREIDING II force field has been fully described in the literature,[44,45] so details of the force field are included as Supporting Information.

The force field was originally parametrized for nickel porphyrins[44] and subsequently extended to other transition metals including zinc,[49] so it could be readily applied to the metal complexes (Ni and Zn) used in our study. The use of the force field to calculate the structures of metal free porphyrins (i.e., free base porphyrins and porphyrin dications) has not been reported in the literature. To calculate the structures of the free base porphyrins and porphyrin dications, hydrogen bonding H atoms were used to represent the inner hydrogen atoms. Counterions were not included in the calculations, and the default charge equilibration scheme[45] was employed. For consistency with earlier studies, the calculations were performed with a dielectric constant of 2.64 (for CS_2). This dielectric constant also reasonably approximates the nonpolar solvents used in the NMR studies (e.g., CD_2Cl_2 or $C_6D_5CD_3$).

The molecular mechanics calculations were divided into two parts. First, the global minimum energy structure was calculated. Then, the aryl group was rotated using a standard dihedral rotation procedure, with the porphyrin being allowed to relax fully at each step of the drive, to obtain the aryl-porphyrin rotational barrier.

Global minimum energy structures and rotational barriers were initially calculated for TArPs **9a** and **9b** using a full range of core substituents (e.g., M = Ni, Zn, 2H or $4H^{2+}$). Similar results were obtained for both porphyrins, so only the data for compound **9b**, which is used in the NMR studies in section III, is discussed. The similarity of both the structures and barriers for TArPs **9a** and **9b** supports the earlier contention that the addition of a *meta* methoxyl substituent results in only a minor structural perturbation. Note that the relative orientation of the methoxyl groups (the atropisomer) was also found to have a negligible effect on the energy minimized structure and on the calculated rotational barrier, so the energy minimized $\alpha\beta\alpha\beta$ atropisomer (which has alternating up and down methoxyl groups) was used as the starting structure for the dihedral rotation.

The global minimum energy structure of **9b** (M = Ni) was found to be modestly ruffled, **9b** (M = Zn) was approximately planar, **9b** (M = 2H) was slightly saddled, and **9b** (M = $4H^{2+}$) was strongly saddled. These results are in general agreement with the crystallographic data for TPP derivatives (Table 3) as they show that nickel(II) favors ruffling of the macrocycle and that protonation induces

(58) Cullen, D. L.; Meyer, E. F. *J. Am. Chem. Soc.* **1974**, *96*, 2095.
(59) This behavior is discussed in a recent paper from our group (ref 73).
(60) Brennan, T. D.; Scheidt, W. R.; Shelnutt, J. A. *J. Am. Chem. Soc.* **1988**, *110*, 3919.
(61) Alden, R. G.; Crawford, B. A.; Doolen, R.; Ondrias, M. R.; Shelnutt, J. A. *J. Am. Chem. Soc.* **1989**, *111*, 2070.
(62) Medforth, C. J.; Berber, M. D.; Smith, K. M.; Shelnutt, J. A. *Tetrahedron Lett.* **1990**, *31*, 3719.
(63) Shelnutt, J. A.; Majumder, S. A.; Sparks, L. D.; Hobbs, J. D.; Medforth, C. J.; Senge, M. O.; Smith, K. M.; Miura, M.; Luo, L.; Quirke, J. M. E. *Raman Spectrosc.* **1992**, *23*, 523.
(64) Hobbs, J. D.; Majumder, S. A.; Luo, L.; Sickelsmith, G. A.; Quirke, J. M. E.; Medforth, C. J.; Smith, K. M.; Shelnutt, J. A. *J. Am. Chem. Soc.* **1994**, *116*, 3261.
(65) Medforth, C. J.; Senge, M. O.; Forsyth, T. P.; Hobbs, J. D.; Shelnutt, J. A.; Smith, K. M. *Inorg. Chem.* **1994**, *33*, 3865.
(66) Sparks, L. D.; Anderson, K. K.; Medforth, C. J.; Smith, K. M.; Shelnutt, J. A. *Inorg. Chem.* **1994**, *33*, 2297.
(67) Jentzen, W.; Hobbs, J. D.; Simpson, M. C.; Taylor, K. K.; Ema, T.; Nelson, N. Y.; Medforth, C. J.; Smith, K. M.; Veyrat, M.; Mazzanti, M.; Ramasseul, R.; Marchon, J.-C.; Takeuchi, T.; Goddard, I. W. A.; Shelnutt, J. A. *J. Am. Chem. Soc.* **1995**, *117*, 11085.
(68) Medforth, C. J.; Hobbs, J. D.; Rodriguez, M. R.; Abraham, R. J.; Smith, K. M.; Shelnutt, J. A. *Inorg. Chem.* **1995**, *34*, 1333.
(69) Song, X.-Z.; Jentzen, W.; Jia, S.-L.; Jaquinod, L.; Nurco, D. J.; Medforth, C. J.; Smith, K. M.; Shelnutt, J. A. *J. Am. Chem. Soc.* **1996**, *118*, 12975.
(70) Jentzen, W.; Unger, E.; Song, X. Z.; Jia, S. L.; Turowska-Tyrk, I.; Schweitzer-Stenner, R.; Dreybrodt, W.; Scheidt, W. R.; Shelnutt, J. A. *J. Phys. Chem. A* **1997**, *101*, 5789.
(71) Song, X.-Z.; Jentzen, W.; Jaquinod, L.; Khoury, R. G.; Medforth, C. J.; Jia, S.-L.; Ma, J.-G.; Smith, K. M.; Shelnutt, J. A. *Inorg. Chem.* **1998**, *37*, 2117.
(72) Nelson, N. Y.; Medforth, C. J.; Nurco, D. J.; Jia, S.-L.; Shelnutt, J. A.; Smith, K. M. *Chem. Commun.* **1999**, 2071.
(73) Haddad, R. E.; Gazeau, S.; Pécaut, J.; Marchon, J.-C.; Medforth, C. J.; Shelnutt, J. A. *J. Am. Chem. Soc.* **2003**, *125*, 1253.

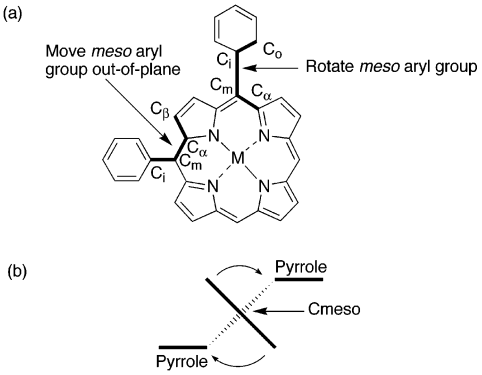

Figure 8. Diagrams showing (a) the torsion angles used in the molecular mechanics calculations of the *meso* aryl rotational barriers and (b) the definition of clockwise rotation of a *meso* aryl group in a saddle deformed porphyrin.

Table 6. Barriers for *meso* 3-Methoxyphenyl Rotation ($\Delta E^{\ddagger}_{ROT}$; kJ mol^{-1}) Obtained from Molecular Mechanics Calculations

porphyrin	$\Delta E^{\ddagger}_{ROT}$
9b (M = Zn)	80[a]
9b (M = Ni)	50[b]
9b (M = 2H)	59[a]
9b (M = 4H^{2+})	51[c]
10b (M = Ni)	58[b]
10b (M = 4H^{2+})	102[b]

[a] Calculated with the rotated *meso* aryl group constained out-of-plane using two $C_\beta-C_\alpha-C_m-C_i$ torsion angles. Rotating the *meso* aryl substituent about the global minimum energy structure gives a higher barrier [88 kJ mol^{-1} for **9b** (M = Zn) and 118 kJ mol^{-1} for **9b** (M = 2H)]. [b] Calculated by rotating the *meso* aryl substituent about the global minimum energy structure. [c] Calculated by rotating the *meso* aryl substituent about the global minimum energy structure. A higher barrier (62 kJ mol^{-1}) is obtained when the rotated *meso* aryl group is constrained out-of-plane using two $C_\beta-C_\alpha-C_m-C_i$ torsion angles.

saddling of the macrocycle. Using the energy minimized $\alpha\beta\alpha\beta$ structure as a starting point, the rotational barriers were then calculated using a dihedral rotation. The $C_\alpha-C_m-C_i-C_o$ torsion angle shown in Figure 8a was used to rotate the aryl group, which was rotated clockwise or counterclockwise in 10° increments with smaller changes around the energy maximum. The rest of the porphyrin structure was allowed to relax fully at each of the steps. The rotational sense of the *meso* aryl group was only found to be important for the saddle structures, and is defined in Figure 8b.

The rotational barriers ($\Delta E^{\ddagger}_{ROT}$) determined from the MM calculations are given in Table 6. For **9b** (M = Ni), the lowest barrier (50 kJ mol^{-1}) was obtained by rotating the aryl group about the minimum energy ruf structure; i.e., rotation occurred when the aryl group was out of the least-squares plane of the porphyrin macrocycle. In contrast, for **9b** (M = 4H^{2+}), the lowest barrier (51 kJ mol^{-1}) was obtained by rotating the aryl group about the minimum energy sad structure, which corresponds to rotation in the plane of the porphyrin macrocycle. The out-of-plane rotation pathway was also investigated for **9b** (M = 4H^{2+}). The out-of-plane pathway was approximated by constraining the aryl substituent to move out-of-plane using two $C_\beta-C_\alpha-C_m-C_i$ torsion angles as shown in Figure 8a. The $C_\alpha-C_m-C_i-C_o$ and $C_\beta-C_\alpha-C_m-C_i$ torsion angles were then varied independently to determine the lowest energy pathway. An optimized $C_\beta-C_\alpha-C_m-C_i$ torsion angle of 50° was found to produce only a slightly higher (62 kJ mol^{-1}) barrier for out-of-plane rotation than for in-plane rotation (51 kJ mol^{-1}). In the case of **9b** (M = Zn), rotating the aryl group in-plane about the minimum energy structure produced a higher barrier (88 kJ mol^{-1}) than that obtained by constraining the $C_\beta-C_\alpha-C_m-C_i$ torsion angles to force the aryl substituent to rotate out-of-plane (80 kJ mol^{-1}). A similar effect was observed for the free base porphyrin **9b** (M = 2H), although in this case the difference between the in-plane (118 kJ mol^{-1}) and out-of-plane (59 kJ mol^{-1}) pathways was much larger. The optimized $C_\beta-C_\alpha-C_m-C_i$ torsion angles for **9b** (M = Zn) and **9b** (M = 2H) (50−55°) were found to be similar to that seen for **9b** (M = 4H^{2+}) (50°).

Overall, the MM calculations correctly predict both the structures and the trends in the experimental rotational barriers for the TArPs.[17−19] A lower barrier is seen for the nickel complex versus the zinc complex of porphyrin **9b** (50 vs 80 kJ mol^{-1}) and also for the dication versus the free base porphyrin (51 vs 59 kJ mol^{-1}). The ordering of the calculated rotational barriers (Ni < 4H^{2+} < 2H < Zn) is also the same as that reported for porphyrin **6**[19] (Table 1).

MM calculations were then performed for TArOPP **10b**, a porphyrin that is used in the NMR studies in section III. Porphyrin **10b** is related to porphyrin **9b** by the addition of phenyl rings to all of the unsubstituted pyrrole positions. Calculations were carried out for porphyrin **10b** with two core substituents: M = Ni, which based on the X-ray data is expected to be the most conformationally flexible system and to adopt sad and/or ruf structures, and M = 4H^{2+}, which is expected to be the least conformationally flexible system because the protons in the core will strongly favor a saddle structure. The global minimum energy structure of **10b** (M = 4H^{2+}) was calculated to be strongly saddle distorted in agreement with the crystal structure of **13e** (M = 4H^{2+}) (Figure 6). Nickel complex **10b** (M = Ni) was also found to have a sad conformation as the global minimum energy structure, although the ruf conformation was also obtained as a stable local minima only 15 kJ mol^{-1} higher in energy than the sad conformation. A stable ruffle conformation could not be obtained for **10b** (M = 4H^{2+}). The finding of sad and ruf conformations of similar energies for the nickel complex of **10b** is consistent with the crystallographic data discussed in section I, which showed both sad and/or ruf conformations for NiDPP (Table 4) and mixed sad/ruf conformations for **13c** (M = Ni) (Figure 5, Table 4).[30,32]

The MM calculations predict a considerable difference in the effect on $\Delta E^{\ddagger}_{ROT}$ of adding eight phenyl rings to porphyrin **9b** to produce porphyrin **10b** for the two core substituents investigated (M = Ni or 4H^{2+}). The lowest barrier for rotation of the 3-methoxyphenyl group in **10b** (M = Ni) was found when the macrocycle was ruffled and the *meso* aryl group moved out of the porphyrin plane. Surprisingly, the calculated barrier (58 kJ mol^{-1}) was only marginally higher than that obtained for **9b** (M = Ni) (50 kJ mol^{-1}) despite the addition of eight phenyl rings to the porphyrin periphery. The lowest barrier for rotation of the 3-methoxyphenyl group in **10b** (M = 4H^{2+}) was much higher

(102 kJ mol^{-1}) and was obtained when the aryl group was rotated clockwise from the saddled minimum energy structure, see Figure 8b, which forced the *meso* aryl group to move out-of-plane. Rotating the *meso* aryl group counterclockwise did not move the aryl group out-of-plane and gave a significantly higher barrier (133 kJ mol^{-1}). The barrier for the dication of **10b** (102 kJ mol^{-1}) was much higher than that calculated for the dication of **9b** (51 kJ mol^{-1}). The barrier for the dication of **10b** (102 kJ mol^{-1}) was also considerably higher than the barrier for the nickel complex of **10b** (58 kJ mol^{-1}).

As noted earlier, an analysis of crystallographic data for the DArPs shows that the C_{ipso}(*meso*)−C(β) and C_{ipso}(*meso*)−C_{ipso}(β) distances are longer in **13e** (M = 4H^{2+}) $(pic)_2$ than in ruf NiDPP (Table 5), implying that the rotational barrier should be lower in the dication. However, the results of the MM calculations in Table 6, which are confirmed by the VT NMR results in section III, indicate that the barrier is actually much higher in the dication than in the nickel complex of TArOPP **10b** (102 versus 58 kJ mol^{-1}). One explanation for the MM results is that the *meso* aryl rotational barrier in TArOPP **10b** is strongly influenced by the deformability along the ruffling coordinate. Ruffling deformation effectively allows the aryl group being rotated to move out of the porphyrin plane to minimize interactions with the rest of the porphyrin (as previously suggested for the metal complexes of TArPs).[17,19] A core substituent which favors or permits ruffling (e.g., nickel) will facilitate the *meso* aryl group moving out-of-plane to minimize aryl−porphyrin interactions and will decrease the rotational barrier. In contrast, a core substituent which disfavors ruffling (such as four protons, where severe steric crowding would occur in the core) will inhibit the aryl group from moving out-of-plane and will increase the rotational barrier.

It should be pointed out that the actual mechanism of aryl rotation in the TArOPPs might be more complicated than that suggested by the MM calculations. For example, rotation of some or all of the aryl groups might be a concerted process. However, the good agreement between the MM and NMR barriers (see section III) plus the fact that we found no evidence of such effects in the MM calculations make this scenario less likely. It is also worth noting that the only time the lowest energy pathway for aryl−porphyrin rotation is not calculated to involve out-of-plane movement of the *meso* aryl group is in the case of **9b** (M = 4H^{2+}). This may be because such a large amount of saddle deformation occurs upon protonation of **9b** (M = 2H), allowing in-plane rotation to compete with out-of-plane rotation in the dication. A related in-plane rotation mechanism may not compete as effectively for the TArOPPs because the dication is so highly substituted.

III. Variable Temperature ^{1}H NMR Spectroscopy. ^{1}H NMR spectra of TArP **9b**, TArOPP **10b**, OArP **11b**, OArTPP **13b**, and DiArTPP **12b** were analyzed as a function of temperature with a view to determining the rotational barriers of the 3-methoxyphenyl substituents in these systems. Activation energies ($\Delta G^{\ddagger}_{ROT}$; kJ mol^{-1}) for rotation of the *meso* 3-methoxyphenyl groups in porphyrins **9b** and **10b**, determined using coalescence data from variable temperature (VT) ^{1}H NMR studies, are provided in Table 7. The corresponding data for the β 3-methoxyphenyl groups in porphyrins **11b**, **12b**, and **13b** are given in Table 8. The porphyrins used in our study are known to display several dynamic processes including NH tautomerism (in the free base porphyrins), substituent rotation (for both the *meso* and β aryl groups), and inversion of the nonplanar macrocycle (TArOPPs and OArTPPs).[43] In an initial study of DPP, we mistakenly assigned one of the dynamic processes for one particular core substituent (M = 4H^{2+}) to macrocyclic inversion instead of β aryl rotation.[26] This error was rectified when additional TArOPPs and OArTPPs were synthesized.[35] In the present study, great care was taken to assign all of the dynamic processes expected for each porphyrin. For example, only one process is expected for **9b** (M = Ni) (*meso* aryl rotation) whereas four processes are expected for **10b** (M = 2H) (NH tautomerism, macrocyclic inversion, *meso* aryl rotation, and β aryl rotation).

Table 7. Activation Energies ($\Delta G^{\ddagger}_{ROT}$; kJ mol^{-1}) and Coalescence Temperatures for *meso* 3-Methoxyphenyl Rotation Obtained from Variable Temperature ^{1}H NMR Studies

porphyrin	M = Zn	M = Ni	M = 2H	M = 4H^{+}
9b	62 ± 2 (273 K)	49 ± 3 (243 K)	45 ± 5[41]	47 ± 2 (218 K)
10b	67 ± 3 (303 K)	55 ± 2 (273 K)	65 ± 3 (288 K)	91 ± 3 (398 K)

Table 8. Activation Energies ($\Delta G^{\ddagger}_{ROT}$; kJ mol^{-1}) and Coalescence Temperatures for β 3-Methoxyphenyl Rotation Obtained from Variable Temperature ^{1}H NMR Studies

porphyrin	M = Zn	M = Ni	M = 2H	M = 4H^{2+}
11b	*a*	*a*	*a*	≥31 ± 3[b]
12b	66 ± 3 (294 K)	65 ± 3 (293 K)	60 ± 4 (273 K)	45 ± 2 (233 K)
13b	52 ± 2 (263 K)	54 ± 3 (251 K)	≥46 ± 2[c]	42 ± 2 (213 K)

[a] Proton NMR spectra showed broadening at low temperatures, but $\Delta G^{\ddagger}$ could not be determined with any degree of accuracy. [b] The dynamic process with $\Delta G^{\ddagger}$ = 31 kJ mol^{-1} might be inversion of the nonplanar porphyrin macrocycle. As aryl−porphyrin rotation must be slow on the NMR time scale rotation to allow inversion to be detected, 31 kJ mol^{-1} is the lower limit for $\Delta G^{\ddagger}_{ROT}$. [c] Atropisomers could be detected when macrocyclic inversion ($\Delta G^{\ddagger}$ = 46 kJ mol^{-1}) was slow on the NMR time scale. As aryl−porphyrin rotation must be slow on the NMR time scale rotation to allow inversion to be detected, this is the lower limit for $\Delta G^{\ddagger}_{ROT}$.

Definitive assignment of the aryl−porphyrin rotation process was achieved by synthesizing porphyrins with aryl groups that were expected to have higher or lower aryl rotation barriers than the 3-methoxyphenyl group. In such a case, the barriers for the other dynamic processes (e.g., NH tautomerism or macrocyclic inversion) were essentially unchanged allowing an unambiguous assignment of the aryl−porphyrin rotation process. Aryl rotation barriers for the porphyrins with the modified aryl groups are given in Table 9. The more bulky 2-methoxyphenyl substituent was found to increase $\Delta G^{\ddagger}_{ROT}$ by approximately 50 kJ mol^{-1} compared to the 3-methoxyphenyl group. The 3-thienyl group was investigated as a way of lowering the rotational barrier and was found to decrease $\Delta G^{\ddagger}_{ROT}$ by approximately 20 kJ mol^{-1} compared to the value for the 3-methoxyphenyl group.

Table 9. Activation Energies ($\Delta G^{\ddagger}_{ROT}$; kJ mol^{-1}) for 3-Thienyl and 2-Methoxyphenyl Rotation Obtained from Variable Temperature ^{1}H NMR Studies

porphyrin	M = Zn	M = Ni	M = 2H	M = 4H^{2+}
8			108[18]	96[18]
13d		≥96[a]		≥84[a]
10c	51 ± 4	44 ± 3	47 ± 2	79 ± 3
12c	*b*	42 ± 3	*b*	*b*
13c	*c*	38 ± 4	30 ± 2	≤27[a]

[a] Estimated from line broadening using the standard equations.[86] [b] Porphyrin could not be prepared (see Experimental Section). [c] Sample was not sufficiently soluble at low temperatures for ^{1}H NMR studies.

The activation energies for 3-methoxyphenyl rotation (Tables 7 and 8) are surprisingly similar given the significant structural differences present among the porphyrins investigated. Most of the barriers fall between 40 and 70 kJ mol^{-1}, with the exception of **10b** (M = 4H^{2+}) where the barrier is much higher as predicted by the MM calculations. Because of the many atropisomers present in the slow exchange spectra, and difficulties in accurately determining the coalescence temperature (T_c) and the slow-exchange chemical shift difference ($\delta\nu$), the errors in the NMR measurements are fairly large (up to 5 kJ mol^{-1}).[74] Despite these limitations, the NMR results for *meso* aryl-substituted porphyrins **9b** and **10b** (Table 7) agree well with the barriers obtained from the MM calculations. Equally importantly, the NMR results support an interpretation based on the deformability of the macrocycle being a significant factor controlling the rotational barriers. This is most clearly illustrated by the barriers for porphyrins **10b** (M = Ni) and **10b** (M = 4H^{2+}) discussed in the following paragraphs, where the difference in $\Delta G^{\ddagger}_{ROT}$ (36 kJ mol^{-1}) is clearly too large to be explained by experimental errors or differences in $\Delta S^{\ddagger}$.[75]

We consider first porphyrins **9b** and **10b** which were investigated in detail in the MM studies in section II. The NMR studies of these porphyrins yield rotational barriers which agree fairly well with those obtained from the MM calculations: **9b** (M = Ni) 49 ± 3 (calcd 50), **9b** (M = 4H^{2+}) 47 ± 2 (calcd 51), **10b** (M = Ni) 55 ± 2 (calcd 58), **10b** (M = 4H^{2+}) 91 ± 3 (calcd 102). The NMR studies verify both the small increase in the rotational barrier predicted for **10b** (M = Ni) versus **9b** (M = Ni) (obsd 6; calcd 8 kJ mol^{-1}) and the much larger increase predicted for **10b** (M = 4H^{2+}) versus **9b** (M = 4H^{2+}) (obsd 44; calcd 51 kJ mol^{-1}). This provides additional support for the argument made in section II that easier deformability along the ruf coordinate lowers the *meso* aryl rotational barriers in the TArOPPs. The rotational barriers for porphyrins **9b** and **10b** with other core substituents are also consistent with this model. A smaller metal (Ni vs Zn) is seen to decrease $\Delta G^{\ddagger}_{ROT}$ by 13 kJ mol^{-1} for **9b** in agreement with earlier studies of TArPs (Table 1).[17−19] A related decrease (12 kJ mol^{-1}) is also seen for **10b** (M = Ni) versus **10b** (M = Zn) and presumably has similar origins, i.e., the ability of the nickel complex to more readily deform along the ruf coordinate and move the *meso* substituent out-of-plane to facilitate rotation (a finding supported by the X-ray data for NiDPP and ZnDPP in section I). On the basis of previous studies of TArPs,[18,19] a lower activation energy for aryl rotation was expected for **9b** (M = 4H^{2+}) versus **9b** (M = 2H), although the barriers were found to be experimentally indistinguishable (Table 7). This may reflect the lower barriers resulting from the less hindered aryl groups in porphyrin **9b** compared to porphyrins **6** and **7**, and the correspondingly greater significance of the experimental error.

The NMR data for the β aryl-substituted porphyrins **11b**, **12b**, and **13b** is incomplete, primarily because of difficulties in accurately measuring the rotational barriers in OArP **11b** (Table 8). However, the barriers which could be measured can be readily interpreted in terms of the out-of-plane deformability model discussed for the TArOPPs. Just as ruffling lowers the barrier for *meso* aryl rotation by moving the *meso* position out-of-plane, so saddling (which moves the pyrrole β positions out-of-plane) appears to lower the barrier for β aryl rotation. Thus, protonation of DiArTPP **12b** (M = 2H) to form a more saddled dication structure is seen to decrease $\Delta G^{\ddagger}_{ROT}$ for the β 3-methoxyphenyl group by approximately 15 kJ mol^{-1}. Note that this is the opposite of the effect seen for the *meso* substituted TArOPP **10b**, where protonation markedly increased the aryl−porphyrin rotational barrier.

In addition, $\Delta G^{\ddagger}_{ROT}$ is found to be lower in OArTPP **13b** than in DiArTPP **12b** irrespective of the core substituent M. This is consistent with the more highly substituted OArTPP being easier to deform along the sad coordinate because of the larger number of peripheral substituents. Put another way, while the immediate environment around the β 3-methoxyphenyl groups is similar in both porphyrins (i.e., a phenyl ring on one side of the ring being rotated and a 3-methoxyphenyl ring on the other side), steric interactions arising from the six additional 3-methoxyphenyl rings in **13b** make it easier to move the β aryl group being rotated out of the porphyrin plane. Interestingly, there is no statistically significant difference in $\Delta G^{\ddagger}_{ROT}$ for DiArTPP **12b** or OArTPP **13b** when a smaller metal (Ni vs Zn) is present (Table 8), although there is for TArP **9b** and TArOPP **10b** (Table 7). This can be explained by the ruffling deformation favored by the nickel atom not moving the β aryl groups out-of-plane in **12b** and **13b**, whereas it does move the *meso* aryl groups out-of-plane in TArP **9b** and TArOPP **10b**.

In summary, the NMR results for the TArOPPs, OArTPPs, and DiArTPPs support the idea that out-of-plane deformability of the macrocycle is important in lowering the activation energy for aryl−porphyrin rotation. Overall, they suggest a straightforward relationship between the position of the aryl substituent being rotated (*meso* or β) and the symmetry of the deformation mode (ruffling or saddling) required to lower the rotational barrier. Ruffling is seen to

(74) Given the complicated nature of the NMR spectra, no attempt was made to perform a detailed simulation and to extract $\Delta H^{\ddagger}$ and $\Delta S^{\ddagger}$.

(75) It seems unlikely that the differences in $\Delta G^{\ddagger}$ could arise solely from the entropic component $\Delta S^{\ddagger}$, as the barriers obtained in our study were generally measured over a small temperature range (see Tables 7 and 8) and previous studies of aryl rotation in TArPs have suggested that $\Delta S^{\ddagger}$ is small (Freitag, R. A.; Whitten, D. G. *J. Phys. Chem.* **1983**, *87*, 3918.).

lower the barrier for *meso* aryl rotation whereas saddling lowers the barrier for β aryl rotation.

Significantly, the peripherally crowded porphyrins investigated in our study reveal some unusual trends in the rotational barriers which are difficult to explain without invoking the deformability model: (1) adding eight phenyl rings to TArP **9b** (M = Ni) to give TArOPP **10b** (M = Ni) produces a very small increase (only 6 kJ mol^{-1}) in the rotational barrier of the *meso* 3-methoxyphenyl substituent (explained using the deformability model by the highly substituted nickel porphyrin being able to ruffle and move the aryl substitutent out of the porphyrin plane to facilitate rotation); (2) adding eight phenyl rings to TArP **9b** (M = $4H^{2+}$) to give TArOPP **10b** (M = $4H^{2+}$) produces a very large increase (44 kJ mol^{-1}) in the rotational barrier of the *meso* 3-methoxyphenyl substituent (because deformation along the ruffling coordinate would result in severe crowding of the four protons in the core, making ruffling distortion highly unfavorable for **10b** (M = $4H^{2+}$)); (3) the rotational barriers are uniformly lower in **13b** than in **12b**, even though the former is more peripherally crowded (this can be understood in terms of the easier deformability of **13b** due to the presence of more substituents).

Finally, it is worth noting that the changes in the dynamic properties of the substituents demonstrated in our study may well be general in nature and independent of the mechanism by which the nonplanar deformation is produced. If this is the case, the nonplanar deformations present in heme proteins[46,76] may also affect the dynamic properties of the porphyrin substituents, provided the deformations are of the correct symmetry.

Experimental Section

X-ray Crystallography. Crystals were grown via solvent diffusion methods using CH_2Cl_2/MeOH for **12c** (M = Ni), $CHCl_3$/MeOH for **13c** (M = Ni), and CH_2Cl_2/cyclohexane for **13e** (M = $4H^{2+}$). X-ray diffraction data were collected on a Bruker SMART 1000 diffractometer with a sealed tube source [λ(Mo Kα) = 0.71073 Å] for **12c** (M = Ni) and **13e** (M = $4H^{2+}$) and on a Siemens P4 diffractometer with a rotating anode source [λ(Cu Kα) = 1.54178 Å] for **13c** (M = Ni). The Bruker SHELXTL V. 5.03 software package was used for structure solution and refinement; scattering factors were used as supplied. Structures were refined based on F^2 using all independent data by full-matrix least-squares methods. Crystallographic data are given in Table 2. Full experimental details, in CIF format, are available as Supporting Information to this article.

Molecular Mechanics Calculations and Normal-Coordinate Structural Decomposition. Full details of the force field used in the molecular mechanics calculations are given as Supporting Information. The normal-coordinate structural decomposition program used to analyze the nonplanar deformations present in the crystal structures has been fully described in the literature,[2,46] and a browser based version is available for general use at http://jasheln.unm.edu.

NMR Spectroscopy. ^{1}H NMR spectra were recorded at a frequency of 300 MHz using sample concentrations of approximately 5 mM. The spectra were referenced to TMS or the solvent signals at 2.09 ppm ($C_6D_5CHD_2$), 5.30 ppm ($CHDCl_2$), 5.94 ppm ($CHCl_2CDCl_2$), or 7.26 ppm ($CHCl_3$). For the variable temperature studies, CD_2Cl_2 or $C_6D_5CD_3$ was typically used as a low temperature solvent and $CDCl_2CDCl_2$ or $C_6D_5CD_3$ as a high temperature solvent. The temperature control unit was calibrated using a published procedure.[77] Unless noted, spectra reported in the Experimental Section were obtained at ambient temperature (293−298 K).

Synthesis. The porphyrins used in the NMR studies were typically prepared in their free base form (M = 2H). Nickel complexes were then prepared by adding $Ni(OAc)_2$ in methanol to the free base porphyrin in refluxing chloroform, or by refluxing a solution of the free base porphyrin in toluene containing $Ni(acac)_2$. Zinc complexes were prepared by adding $Zn(OAc)_2$ in methanol to the free base porphyrin in refluxing chloroform. The metal complexes were purified by recrystallization from dichloromethane by addition of methanol. The dications were prepared in situ prior to the NMR experiments by addition of 1 vol % of trifluoroacetic acid to the free base porphyrins. Visible spectra absorption maxima and absorption coefficients were recorded on either a Hewlett-Packard 8450A diode array spectrophotometer or a Hewlett-Packard 8452A diode array spectrometer using CH_2Cl_2 as solvent for the nickel or zinc complexes, 99% CH_2Cl_2/1% $N(CH_3CH_2)_3$ for the free base porphyrins, and 99% CH_2Cl_2/1% CF_3CO_2H for the dications. Mass spectral analyses were generally performed using matrix-assisted laser desorption/ionization Fourier transform mass spectrometry (MALDI-FTMS) in the positive ion detection mode as described previously.[78] Some mass spectra were obtained using LSIMS at the Mass Spectrometry Facility at the University of California, San Francisco. Melting points (uncorrected) were measured on a Thomas/Bristoline microscopic hot stage apparatus.

5,10,15,20-Tetrakis(3-methoxyphenyl)porphyrin [9b (M = 2H)]. The synthesis of this porphyrin has been reported previously.[41] **9b** (M = 2H). ^{1}H NMR (CD_2Cl_2): 8.88 (s, 8H, H_β), 7.79 (d, 4H, H_6), 7.76 (s, 4H, H_2), 7.64 (t, 4H, H_5), 7.33 (m, 4H, H_4), 3.96 (s, 24H, OCH_3), −2.9 (s, 2H, NH). **9b** (M = $4H^{2+}$). ^{1}H NMR (CD_2Cl_2 + 1% CF_3CO_2H): 8.77 (s, 8H, H_β), 8.13 (s, 4H, H_2), 8.11 (d, 4H, H_6), 7.92 (t, 4H, H_5), 7.57 (m, 4H, H_4), 4.15 (s, 24H, OCH_3), −1.3 (s, 4H, NH). **9b** (M = Ni). ^{1}H NMR (CD_2Cl_2/CS_2 1:4 by volume): 8.73 (s, 8H, H_β), 3.94 (s, 24H, OCH_3). The sample was too dilute to reliably assign other signals from the 3-methoxyphenyl group. **10b** (M = Zn). ^{1}H NMR (CD_2Cl_2): 8.96 (s, 8H, H_β), 7.78 (d, 4H, H_6), 7.73 (s, 4H, H_2), 7.63 (t, 4H, H_5), 7.29 (m, 4H, H_4), 3.92 (s, 24H, OCH_3).

5,10,15,20-Tetrakis(3-methoxyphenyl)-2,3,7,8,12,13,17,18-octaphenylporphyrin [10b (M = 2H)]. This compound was obtained as green crystals in 11% yield from the condensation of 3,4-diphenylpyrrole with 3-methoxybenzaldehyde using a modified Adler−Longo procedure.[42] **10b** (M = 2H). Mp: >300 °C. MALDI-FTMS [M + H]: 1343.5, calculated 1343.5. ^{1}H NMR (CD_2Cl_2): 7.22 (br, 4H, aryl-H_6), 7.11 (br, 4H, aryl-H_2), 6.73 (br, 44H, phenyl-H and aryl-H_5), 6.34 (m, 4H, aryl-H_4), 3.67 (s, 12H, OCH_3), NH signal not observed. Visible spectrum (CH_2Cl_2 + 1% $N(C_2H_5)_3$), λ/nm (ϵ/cm^{-1} mol^{-1} dm^{-3}): 466 (234 000), 562 (25 800), 614 (24 200), 712 (16 400). **10b** (M = $4H^{2+}$). ^{1}H NMR (CD_2Cl_2 + 1% CF_3CO_2H): 7.51−7.70 (8H, aryl-H_2 and H_6), 7.04−7.10 (4H, meso-H_5), 6.65−6.85 (44H, phenyl-H and aryl-H_4), 3.82−3.87 (24H, OCH_3), NH signal not observed. Visible spectrum (CH_2Cl_2 + 1% CF_3COOH), λ/nm (ϵ/cm^{-1} mol^{-1} dm^{-3}): 496 (196 000), 720 (43 600). **10b** (M = Ni). Mp: >300 °C. ^{1}H NMR (CD_2Cl_2): 6.60−

(76) Jentzen, W.; Ma, J. G.; Shelnutt, J. A. *Biophys. J.* **1998**, *74*, 753.

(77) van Geet, A. L. *Anal. Chem.* **1970**, *42*, 679.

(78) Green, M. K.; Medforth, C. J.; Muzzi, C. M.; Nurco, D. J.; Shea, K. M.; Smith, K. M.; Shelnutt, J. A.; Lebrilla, C. B. *Eur. Mass Spectrom.* **1997**, *3*, 439.

6.74 (br, 52H, phenyl-H and aryl-H_2, H_5, and H_6), 6.23 (m, 4H, aryl-H_4), 3.47 (br s, 12H, OCH_3). Visible spectrum (CH_2Cl_2), λ/nm (ϵ/cm^{-1} mol^{-1} dm^{-3}): 448 (100 000), 566 (7900), 610 (8800). **10b** (M = Zn). ^{1}H NMR (CD_2Cl_2): 6.7−7.2 (br, 52H, phenyl-H and aryl-H_2, H_5, and H_6), 6.28 (m, 4H, aryl-H_4), 3.61 (s, 12H, OCH_3).

2,3,7,8,12,13,17,18-Octaphenyl-5,10,15,20-tetrakis(3-thienyl)-porphyrin [10c (M = 2H)]. This compound was obtained as brown crystals in 19% yield from the condensation of 3,4-diphenylpyrrole with thiophene-3-carboxaldehyde using a modified Adler−Longo reaction.[42] **10c** (M = 2H). Mp: >300 °C. LSIMS [M + H]: 1248.2, calculated 1247.3. ^{1}H NMR (CD_2Cl_2): 7.34 (br s, 4H, thienyl-H_2), 7.12 (m, 4H, thienyl-H_5), 6.81 (br, 40H, phenyl-H), 6.57 (m, 4H, thienyl-H_4), −1.00 (br s, 2H, NH). Visible spectrum (CH_2Cl_2 + 1% $N(C_2H_5)_3$), λ/nm (ϵ/cm^{-1} mol^{-1} dm^{-3}): 470 (184 000), 572 (10 800), 622 (13 300), 728 (7000). **10c** (M = 4H^{2+}). ^{1}H NMR (CD_2Cl_2 + 1% CF_3CO_2H): 7.87 (br, 4H, thienyl-H_2), 7.56 (br, 4H, thienyl-H_5), 6.71−6.96 (m, 44H, phenyl-H and thienyl-H_4). Visible spectrum (CH_2Cl_2 + 1% CF_3COOH), λ/nm (ϵ/cm^{-1} mol^{-1} dm^{-3}): 496 (170 000), 740 (44 100). **10c** (M = Ni). Mp: >300 °C. ^{1}H NMR (CD_2Cl_2): 6.79 (m, 40H, phenyl-H), 6.68 (m, 4H, thienyl-H_2), 6.52 (m, 4H, thienyl-H_5), 6.23 (m, 4H, thienyl-H_4). Visible spectrum (CH_2Cl_2), λ/nm (ϵ/cm^{-1} mol^{-1} dm^{-3}): 450 (200 000), 568 (17 300), 612 (16 200). **10c** (M = Zn). ^{1}H NMR (CD_2Cl_2): 6.78 (m, 40H, phenyl-H), 7.15 (m, 4H, thienyl-H_2), 7.00 (m, 4H, thienyl-H_5), 6.45 (m, 4H, thienyl-H_4).

2,3,7,8,12,14,17,18-Octakis(3-methoxyphenyl)porphyrin [11b (M = 2H)]. This compound was isolated as a light brown powder in 10% yield from the condensation of 3,4-bis(3-methoxyphenyl)-pyrrole with formaldehyde using a modification of a published procedure.[48] 3,4-Bis(3-methoxyphenyl)pyrrole was prepared from 3,3′-dimethoxybenzil and dimethyl-*N*-acetyliminodiacetate.[79] 3,3′-Dimethoxybenzil was obtained by condensing 3-methoxybenzaldehyde to form the benzoin[80] and then oxidizing the benzoin to the corresponding benzil.[81] **11b** (M = 2H). MALDI-FTMS [M + H]: 1159.2, calculated 1159.5. ^{1}H NMR (CD_2Cl_2): 10.38 (s, 4H, H_{meso}), 7.60 (s, 8H, H_6), 7.55 (d, 8H, H_2), 7.54 (t, 8H, H_5), 7.11 (m, 8H, H_4), 3.82 (s, 24H, OCH_3), −3.1 (s, 2H, NH). Visible spectrum (CH_2Cl_2), λ/nm: 419, 512, 549, 578, 632. **7** (M = 4H^{2+}). **11b** (M = 4H^{2+}). ^{1}H NMR (CD_2Cl_2 + 1% CF_3CO_2H): 10.77 (s, 4H, H_{meso}), 7.57 (t, 8H, H_5), 7.44 (s, 8H, H_2), 7.43 (d, 8H, H_6), 7.19 (m, 8H, H_4), 3.81 (s, 24H, OCH_3), −2.5 (s, 4H, NH) (at 203 K). **11b** (M = Ni). ^{1}H NMR (CD_2Cl_2): 10.04 (s, 4H, H_{meso}), 7.47 (t, 8H, H_5), 7.43 (d, 8H, H_6), 7.38 (s, 8H, H_2), 7.05 (d, 8H, H_4), 3.78 (s, 24H, OCH_3). **11b** (M = Zn). ^{1}H NMR (CD_2Cl_2): 10.45 (s, 4H, H_{meso}), 7.63 (d, 8H, H_6), 7.55 (s, 8H, H_2), 7.53 (t, 8H, H_5), 7.08 (m, 8H, H_4), 3.80 (s, 24H, OCH_3).

2,3-Bis(3-methoxyphenyl)-5,10,15,20-tetraphenylporphyrin [12b (M = Ni)]. This compound was isolated as blue crystals in 38% yield from the Suzuki coupling reaction[82,83] of nickel(II)-2,3-dibromotetraphenylporphyrin[84] with 3-methoxyphenylboronic acid. The porphyrin was demetalated by treatment with concentrated sulfuric acid for 20 min. **12b** (M = Ni). Visible spectrum (CH_2Cl_2), λ/nm (ϵ/cm^{-1} mol^{-1} dm^{-3}): 422 (221 000), 538 (14 700) ^{1}H NMR ($CDCl_3$): 8.69 (s, 2H, $H_{12,13}$), 8.57 (d, 2H, $H_{8,17}$), 8.37 (d, 2H, $H_{7,18}$), 7.98 (d, 4H, 10,15-H_{ortho}), 7.66 (m, 6H, 10,15-H_{meta} and H_{para}), 7.49 (d, 4H, 5,20-H_{ortho}), 7.20 (t, 2H, 5,20-H_{para}), 7.09 (t, 4H, 5,20-H_{meta}), 6.77 (t, 2H, aryl-H_5), 6.49 (m, 4H, aryl-H_4 and H_6), 6.35 (s, 2H, aryl-H_2), 3.54 (s, 6H, OCH_3). **12b** (M = 2H). ^{1}H NMR ($CDCl_3$): 8.80 (s, 2H, $H_{12,13}$), 8.71 (d, 2H, $H_{8,17}$), 8.57 (d, 2H, $H_{7,18}$), 8.21 (d, 4H, 10,15-H_{ortho}), 7.82 (m, 6H, 10,15-H_{meta} and H_{para}), 7.28 (d, 4H, 5,20-H_{ortho}), 7.24 (m, 6H, 5,20-H_{meta} and H_{para}), 6.79 (t, 2H, aryl-H_5), 6.53 (m, 4H, aryl-H_2 and H_6), 6.46 (m, 2H, aryl-H_4), 3.61 (s, 6H, OCH_3), −2.5 (s, 2H, NH). **12b** (M = 4H^{2+}). ^{1}H NMR ($CDCl_3$ + 1% CF_3CO_2H): 8.68 (s, 2H, $H_{12,13}$), 8.53 (m, 4H, 10,15-H_{ortho}), 8.50 (d, 2H, $H_{8,17}$), 8.38 (d, 2H, $H_{7,18}$), 8.20 (m, 4H, 5,20-H_{ortho}), 8.00 (m, 6H, 10,15-H_{meta} and H_{para}), 7.58 (m, 6H, 5,20-H_{meta} and H_{para}), 6.81 (t, 2H, aryl-H_5), 6.53 (m, 2H, aryl-H_4), 6.4 (m, 4H, aryl-H_2 and H_6), 3.55 (s, 6H, OCH_3), −2.1 (s, 4H, NH). **12b** (M = Zn). ^{1}H NMR ($CDCl_3$): 8.85 (d, 2H, $H_{8,17}$), 8.65 (s, 2H, $H_{12,13}$), 8.65 (d, 2H, $H_{7,18}$), 7.78 (d, 4H, 5,20-H_{ortho}), 7.72 (d, 4H, 10,15-H_{ortho}), 7.69 (m, 6H, 10,15-H_{meta} and H_{para}), 7.50 (m, 6H, 5,20-H_{meta} and H_{para}), 6.79 (t, 2H, aryl-H_5), 6.60 (s, 2H, aryl-H_2), 6.55 (m, 2H, aryl-H_6), 6.46 (m, 2H, aryl-H_4), 3.62 (s, 6H, OCH_3).

5,10,15,20-Tetraphenyl-2,3-bis(3-thienyl)porphyrin [12c (M = Ni)]. This compound was obtained as purple crystals in 33% yield from the Suzuki coupling reaction[82,83] of nickel(II)-2,3-dibromotetraphenylporphyrin[84] with thiophene-3-boronic acid. The porphyrin decomposed when demetalation was attempted. **12c** (M = Ni). Visible spectrum (CH_2Cl_2), λ/nm (ϵ/cm^{-1} mol^{-1} dm^{-3}): 422 (226 000), 500 (6300), 537 (23 600). ^{1}H NMR (CD_2Cl_2): 8.66 (s, 2H, $H_{12,13}$), 8.55 (d, 2H, $H_{8,17}$), 8.37 (d, 2H, $H_{7,18}$), 7.96 (d, 4H, 10,15-H_{ortho}), 7.66 (m, 6H, 10,15-H_{meta} and H_{para}), 7.52 (d, 4H, 5,-20-H_{ortho}), 7.22 (m, 6H, 5,20-H_{para}, H_{meta}), 6.79 (m, 2H, thienyl-H_4), 6.63 (m, 4H, thienyl-H_2), 6.50 (m, 2H, thienyl-H_5).

2,3,7,8,12,13,17,18-Octakis(3-methoxyphenyl)-5,10,15,20-tetraphenylporphyrin [13b (M = 2H)]. This compound was obtained as purple crystals in 43% yield using the Suzuki coupling reaction[82,83] of **2** (M = 2H)[85] with 3-methoxyphenylboronic acid. **13b** (M = 2H). Mp: 260−263 °C. MALDI-FTMS [M + H]: 1463.6, calculated 1463.6. ^{1}H NMR ($CDCl_3$): 7.63 (d, 8H, phenyl-H_{ortho}), 6.82 (m, 12H, phenyl-H_{meta} and H_{para}), 6.61 (t, 8H, aryl-H_5), 6.37 (br, 8H, aryl-H_6), 6.29 (m, 8H, aryl-H_4), 6.23 (br, 8H, aryl-H_2), 3.50 (s, 24H, OCH_3), NH signal not observed. Visible spectrum (CH_2Cl_2 + 1% $N(C_2H_5)_3$), λ/nm (ϵ/cm^{-1} mol^{-1} dm^{-3}): 468 (210 000), 566 (13 900), 620 (13 900), 728 (8100). **13b** (M = 4H^{2+}). ^{1}H NMR (CD_2Cl_2 + 1% CF_3CO_2H): 8.05 (m, 8H, phenyl-H_{ortho}), 7.18 (m, 12H, phenyl-H_{meta} and H_{para}), 6.69 (t, 8H, aryl-H_5), 6.39 (m, 8H, aryl-H_4), 6.29 (br, 8H, aryl-H_2), 6.25 (br, 8H, aryl-H_6), 3.50 (s, 24H, OCH_3), NH signal not observed. **13b** (M = Ni). ^{1}H NMR (CD_2Cl_2): 7.04 (br, 8H, phenyl-H_{ortho}), 6.72 (t, 4H, phenyl-H_{para}), 6.61 (br, 16H, phenyl-H_{meta} and aryl-H_5), 6.29 (d, 8H, aryl-H_4), 6.2−6.4 (br, 16H, aryl-H_2 and H_6), 3.45 (s, 24H, OCH_3). Visible spectrum (CH_2Cl_2), λ/nm (ϵ/cm^{-1} mol^{-1} dm^{-3}): 448 (203 000), 568 (16 500), 612 (17 800). **13b** (M = Zn). ^{1}H NMR (CD_2Cl_2): 7.53 (br, 8H, phenyl-H_{ortho}), 6.78 (t, 4H, phenyl-H_{para}), 6.69 (t, 8H, phenyl-H_{meta}), 6.55 (t, 8H, aryl-H_5), 6.23 (m, 24H, aryl-H_2, H_4 and H_6), 3.54 (s, 24H, OCH_3).

5,10,15,20-Tetraphenyl-2,3,7,8,12,13,17,18-octakis(3-thienyl)-porphyrin [13c (M = 2H)]. This compound was obtained as brown/green crystals in 20% yield from the Suzuki coupling reaction[82,83] of **2** (M = 2H)[85] with thiophene-3-boronic acid. **13c** (M = 2H). Mp: >300 °C. MALDI-FTMS [M + H]: 1271.9,

(79) Friedman, M. *J. Org. Chem.* **1965**, *30*, 859.
(80) Williamson, K. L. *Macroscale and Microscale Organic Experiments*; D. C. Heath and Co.: Lexington, MA, 1989; p 534.
(81) Wilcox, C. F. J. *Experimental Organic Chemistry, A Small Scale Approach*; MacMillan Publishing Co.: New York, 1988; p 427.
(82) Chan, K. S.; Zhou, X.; Luo, B.-S.; Mak, T. C. W. *J. Chem. Soc., Chem. Commun.* **1994**, 271.
(83) Zhou, X.; Zhou, Z.; Mak, T. C. W.; Chan, K. S. *J. Chem. Soc., Perkin Trans. 1* **1994**, 2519.
(84) Jaquinod, L.; Khoury, R. G.; Shea, K. M.; Smith, K. M. *Tetrahedron* **1999**, *55*, 13151.
(85) Bhyrappa, P.; Krishnan, V. *Inorg. Chem.* **1991**, *30*, 239.
(86) Abraham, R. J.; Fisher, J.; Loftus, P. *Introduction to NMR Spectroscopy*; Wiley: Chichester, U.K., 1988.

calculated 1271.2. ^{1}H NMR (CD_2Cl_2): 7.81 (m, 8H, phenyl-H_{ortho}), 7.03 (m, 12H, phenyl-H_{meta} and $-H_{para}$), 6.64 (m, 8H, thienyl-H_4), 6.57 (br, 8H, thienyl-H_2), 6.40 (br, 8H, thienyl-H_5), −0.80 (br s, 2H, NH). Visible spectrum (CH_2Cl_2 + 1% $N(C_2H_5)_3$), λ/nm (ϵ/cm^{-1} mol^{-1} dm^{-3}): 478 (98 700), 570 (8100), 622 (8000), 730 (3400). **13c** (M = $4H^{2+}$). ^{1}H NMR (CD_2Cl_2 plus 1% CF_3CO_2H): 8.15 (m, 8H, phenyl-H_{ortho}), 7.29 (m, 12H, phenyl-H_{meta} and -H_{para}), 6.72 (m, 8H, thienyl-H_4), 6.63 (m, 8H, thienyl-H_2), 6.41 (m, 8H, thienyl-H_5), NH signal not observed. Visible spectrum (CH_2Cl_2 + 1% CF_3COOH), λ/nm (ϵ/cm^{-1} mol^{-1} dm^{-3}): 506 (76 200), 740 (22 500). **13c** (M = Ni). ^{1}H NMR (CD_2Cl_2): 7.16 (m, 8H, phenyl-H_{ortho}), 6.90 (m, 12H, phenyl-H_{para}), 6.78 (m, 8H, phenyl-H_{meta}), 6.60 (m, 8H, thienyl-H_4), 6.44 (m, 8H, thienyl-H_2), 6.25 (m, 8H, thienyl-H_5). Visible spectrum (CH_2Cl_2), λ/nm (ϵ/cm^{-1} mol^{-1} dm^{-3}): 454 (182 000), 570 (14 400), 618 (18 100). **13c** (M = Zn). ^{1}H NMR (CD_2Cl_2): 7.68 (m, 8H, phenyl-H_{ortho}), 6.93 (m, 12H, phenyl-H_{para} and H_{meta}), 6.60 (m, 8H, thienyl-H_4), 6.44 (m, 8H, thienyl-H_2), 6.27 (m, 8H, thienyl-H_5).

2,3,7,8,12,13,17,18-Octakis(2-methoxyphenyl)-5,10,15,20-tetraphenylporphyrin [13d (M = 2H)]. This compound was obtained as brown/green crystals in 14% yield from the Suzuki coupling reaction[82,83] of **2** (M = 2H)[85] with 2-methoxyphenylboronic acid. **13d** (M = 2H). Mp: >300 °C. MALDI-FTMS [M + H]: 1463.6, calculated 1463.6. ^{1}H NMR (CD_2Cl_2): 6.1−7.6 (52H, aromatic protons), 2.8−3.7 (24H, OCH_3), NH signal not observed. Visible spectrum (CH_2Cl_2 + 1% N $(C_2H_5)_3$), λ/nm (ϵ/cm^{-1} mol^{-1} dm^{-3}): 452 (187 000), 546 (1900), 596 (12 800), 625 (10 000), 692 (7100). **13d** (M = $4H^{2+}$). ^{1}H NMR ($CDCl_3$ + 1% CF_3CO_2H): 5.4−8.2 (52H, aromatic protons), 2.4−2.6 (pseudoaxial OCH_3), 3.6−3.9 (pseudoequatorial OCH_3), NH signal not observed. Visible spectrum (CH_2Cl_2 + 1% CF_3COOH), λ/nm (ϵ/cm^{-1} mol^{-1} dm^{-3}): 484 (92 600), 712 (23 800). **13d** (M = Ni). Mp: >300 °C. ^{1}H NMR (CD_2Cl_2): 5.9−7.8 (52H, aromatic protons), 3.0−3.5 (24H, OCH_3). Visible spectrum (CH_2Cl_2), λ/nm (ϵ/cm^{-1} mol^{-1} dm^{-3}): 442 (136 000), 562 (16 300), 602 (9600).

2,3,7,8,12,13,17,18-Octakis(4-fluorophenyl)-5,10,15,20-tetraphenylporphyrin [13e (M = 2H)]. The synthesis of this porphyrin has been reported previously.[34] The picrate salt used in the crystal structure determination of **13e** (M = $4H^{2+}$) was prepared by washing a solution of **13e** (M = 2H) in CH_2Cl_2 with a saturated aqueous solution of picric acid. The organic layer was then separated and dried by filtration through anhydrous sodium sulfate and the solvent removed under vacuum.

Acknowledgment. This work was supported by grants from the National Institutes of Health (HL 22252) and the National Science Foundation (CHE-99-04076). This work was partially supported by the Division of Materials Sciences and Engineering, Office of Basic Sciences, U.S. Department of Energy. Sandia is a multiprogram laboratory operated by Sandia Corporation, a Lockheed-Martin company, for the United States Department of Energy under Contract DE-ACO4-94AL85000. Mass spectrometric analyses were performed by the UCSF Mass Spectrometry Facility (A. L. Burlingame, Director) supported by the Biomedical Research Technology Program of the National Center for Research Resources, NIH NCRR BRTP 01614.

Supporting Information Available: X-ray crystallographic files in CIF format for porphyrins **12c** (M = Ni), **13c** (M = Ni), and **13e** (M = $4H^{2+}$). Full details of the force field used in the molecular mechanics calculations. This material is available free of charge via the Internet at http://pubs.acs.org.

IC010958A